CORA Cork Open Research Archive
Cartlann Taighde Oscailte Chorcaí

Title	Determination of composition distributions of multi-particle crystalline samples by sequential dissolution with concomitant particle sizing and solution analysis
Authors	Moynihan, Humphrey A.;Armstrong, Declan
Publication date	2018-04-01
Original Citation	Moynihan, H. A. and Armstrong, D. (2018) 'Determination of composition distributions of multi-particle crystalline samples by sequential dissolution with concomitant particle sizing and solution analysis', CrystEngComm, 20(18), pp. 2617-2633. DOI: 10.1039/C8CE00206A
Type of publication	Article (peer-reviewed)
Link to publisher's version	http://pubs.rsc.org/en/content/articlehtml/2018/ce/c8ce00206a - 10.1039/C8CE00206A
Rights	© The Royal Society of Chemistry 2018. This is the Accepted Manuscript version of a published work that appeared in final form in CrystEngCommon.To access the final published version of record, see http://pubs.rsc.org/en/content/articlehtml/2018/ce/c8ce00206a
Download date	2026-10-30 05:02:12
Item downloaded from	https://hdl.handle.net/10468/6453



University College Cork, Ireland
Coláiste na hOllscoile Corcaigh

Determination of composition distributions of multi-particle crystalline samples by sequential dissolution with concomitant particle sizing and solution analysis

Humphrey A. Moynihan* and Declan Armstrong

School of Chemistry / Analytical and Biological Chemistry Research Facility / Synthesis and Solid-state Pharmaceutical Centre, University College Cork, College Road, Cork, TY12 YN60, Republic of Ireland.

h.moynihan@ucc.ie

Keywords: pharmaceutical impurities, solid solutions, dissolution

Abstract: Impurities arise in the production of molecular pharmaceutical and fine chemical products and are often addressed by crystallisation. However, impurities are not always adequately removed by crystallisations and in some cases impurities are to a certain extent incorporated within crystal particles. The present work aims to develop approaches to mapping the distribution of impurities within crystal particles for samples of multiple particles by controlled stepwise dissolution in conjunction with analysis by HPLC and sizing of the crystals. 2-Nitro-4-trifluoromethylacetanilide (**1**) was selected as the compound for study while 4-methyl-2-nitroacetanilide (**2**), 4-chloro-2-nitroacetanilide (**3**) and *N*-(2-nitro-4-trifluoromethylphenyl)pivalamide (**4**) were selected as the added impurities. The degree of incorporation of additives **2**, **3** and **4** into crystals of compound **1** grown from solutions containing up to 10% of the additive was determined, using 50% aqueous ethanol and toluene as solvents. The stepwise dissolution of samples of crystals of compound **1** in hexane, in which compound **1** has low solubility, containing 2-(2-ethylhexyloxy)ethanol to inhibit flocculation, showed reasonably even dissolution of all crystal particles. Analysis of the resulting solutions by HPLC gave composition data which could be assigned to averaged dissolution regions of the crystals, generating distributions of the level of each additive throughout the crystal particle, these being found to be relatively even for additive **2** and **3**, and uneven for additive **4**.

Introduction

The composition of a crystalline material, i.e. the identity and number of components, is generally considered to be relatively uniform. However, in certain cases, the composition of crystalline materials may not be perfectly uniform. Presence of impurities in crystalline solids

is a significant feature of many materials and technologies.[1,2,3] Impurities in molecular solids are a common occurrence in the manufacturing scale synthesis of many pharmaceuticals and fine chemicals.[4] Such impurities may arise from residual starting materials, reaction by-products, intermediate products, reagents, solvents, catalyst ligands or stereoisomers. For pharmaceuticals in particular, regulations exist concerning the nature and acceptable levels of impurities.[5,6] Crystallisations are often the key unit processes involved in management of impurities.[4] The utility of crystallisation from solution as a method of purification lies in the selectivity of the processes of crystal nucleation and growth for the components of the crystal lattice, while other components present in the system, i.e. impurities, selectively remain in the mother liquor. The relative quantities of crystallising compound and impurities present in solution, their relative solubilities and lattice compatibilities, and the yield of the crystallisation are key factors in achieving successful purification.[7,8] There are reported cases where a crystallisation step can reduce the levels of some but not all impurities to acceptable levels.[9] In cases where a crystallisation does not acceptably reduce the level of a particular impurity, successful purification may occur in conjunction with a phase transformation giving a different crystal form which better rejects the impurity.[10,11,12] In some cases, the process chemistry may need to be further refined so as to reduce the quantity of impurity formed in advance of purification by crystallisation.[13-18] The efficiency of washing during isolation and filtration of the crystalline mass is also important in achieving purity specification.[19,20] In addition to being a method of purification, process scale crystallisation also often acts as a method of product isolation and as a preliminary method for control of particle properties such as crystal form and particle size distribution; presence of impurities can also have profound effects on these outcomes.[21-27]

In many cases, crystallisation processes do not adequately decrease the level of specific impurities at all or without significant further process optimisation.[9,13-18,28-29] A question which arises in such cases concerns the location or locations of the impurity compounds within the crystalline batch. In cases in which certain impurities cannot be adequately removed by crystallisation and the failure cannot be addressed by improved crystal growth or washing, the likelihood is high that impurity compounds are in some way contained within the bulk crystal particles. Impurity content is generally measured as a property of a sample as a whole, for example, by dissolving the sample and analysing the resulting solution by HPLC. Such an approach provides the overall level of a specific impurity in a sample, typically as a percentage of the total composition. However, as outlined above, the behaviour of impurities during

crystallisation processes can vary considerably, suggesting that it cannot be assumed that the distribution of a specific impurity within a batch of crystals is either uniform or localised. It would be safer to assume that, in general, the concentration of a specific impurity may vary, both within crystal particles and between particles. Ideally, impurity concentrations would be determined in a manner which allows evaluation of such a distribution of impurity levels within and between particles.

Some workers have attempted to measure the distributions of impurities within crystals.[30,31,32] For example, careful sequential dissolution and analysis studies on individual L-asparagine monohydrate crystals, grown from solutions in which other amino acids were also present, showed that most amino acid impurities that were incorporated were largely located on the outer or surface layers of the crystals.[33] Preparation of phenacetin by *O*-ethylation of 4-hydroxyacetanilide was found to give unreacted starting material and the competing *N*-ethyl analogue as impurities; the latter was easily purged by recrystallisation whereas the former could not be fully removed in this way. Careful sequential dissolution studies on carefully grown single crystals of phenacetin showed that the 4-hydroxyacetanilide impurity was present in varying concentration throughout the crystal particles.[34] Other impurities structurally similar to and possessing the same supramolecular binding motifs as phenacetin were likewise found to be present throughout phenacetin crystals.[4]

This approach points a possible way towards determining the impurity content of crystals both in terms of overall levels of specific impurities but also in terms of the distribution of those impurities within crystals. It would be expected that impurities located at the surface or outer portions of crystal particles would be more readily removable by washing or recrystallization, while those distributed throughout crystal particles may require a phase transformation or process optimization to effect removal. Methods which would allow the routine determination of the distribution of impurities within batches of crystalline particles would be valuable in guiding impurity management in process design. The present study aims to present a simple approach toward the controlled partial dissolution of a multi-particle crystalline sample, with analysis of the resulting solutions providing data on composition, and particle sizing providing data of the locations of the samples to which that data pertains. This will be carried out using a crystalline system for which the crystallizing molecules can readily be substituted, so as to provide samples in which impurities are reasonably distributed throughout, while controlled dissolution will be provided by suitable choice of solvent medium and inhibition of particle agglomeration.

Experimental Methods

Materials

HPLC grade solvents such as acetonitrile and deionised water were purchased from the Honeywell CHROMASOLV Plus range. All other reagents and solvents were obtained from commercial suppliers and used without further purification. The synthesis of *N*-(2-nitro-4-trifluoromethylphenyl)pivalamide (**4**) is described in the Supplementary Information. The compounds 2-nitro-4-trifluoromethylacetanilide (**1**), 4-methyl-2-nitroacetanilide (**2**), and 4-chloro-2-nitroacetanilide (**3**) were prepared according to previously reported methods.[32,35,36]

High-performance liquid chromatography

Data was obtained from an Agilent 1290 Infinity II LC System interfaced to a Dell OptiPlex 5040. A reverse-phase C-18 column (5 μm, length 250 mm, i.d. 2.0 mm, Varian Polaris C18-A2000250X020) was used to separate compounds **1**, **2**, **3**, and **4**. The mobile phase consisted of 67.5:32.5 water:acetonitrile for 0 - 14.5 minutes with a flow rate of 0.45 mL/min, graduating to 45:55 water:acetonitrile at 14.5 - 16.5 minutes, and then at 45:55 water:acetonitrile for 16.5 - 24.8 minutes with a flow rate of 0.5 mL/min. The injection volume was 5 μL and the detector was set at 234 nm. Good baseline resolutions were obtained for all compounds eluting at 23.28, 12.75, 7.00 and 5.07 min for **4**, **1**, **3**, and **2** respectively. Calibration curves were constructed for approximate compound concentrations of 100, 50, 25, 10, 5, 2.5, and 1 μg/mL (see Supplementary Information).

Solubility

Solubility measurements were obtained by first dissolving the desired compound in the solvent of choice at a set temperature in an oil bath until further additions of the investigated compound formed a sustained suspension of material. Once a saturated solution had formed the flask contents were stirred for a further 15 minutes to allow for solvent equilibration. The flask contents were then filtered quickly through a 0.22 μm membrane filter (Kinesis, PVDF). The filtrate was then stirred for 15 minutes at the previously set temperature to allow for solvent equilibration. Three 1 mL or 0.5 mL volumes were drawn from this solution by micropipette and transferred to pre-weighed sample vials. The solvent from these samples vials was allowed to evaporate in a fumehood with further drying of the sample vials under high vacuum. The

weight of the sample vials' contents were determined and the average of three measurements were used to calculate the solubility.

Crystallisation of 2-nitro-4-trifluoromethylacetanilide **1** with additives

Samples of **1** containing additives **2**, **3**, or **4** were prepared with additive levels ranging from 0.5 mol % to 10 mol %. Stock solutions of **1** and the additives were prepared in diethyl ether, and the appropriate volumes of the two solutions were mixed to acquire target doping levels. The diethyl ether solvent was allowed to evaporate overnight in a fumehood and the residues were further dried under high vacuum. The appropriate amount of crystallisation solvent was added to the residues, the samples were heated to ~80 °C with swirling of the sample vials to assist dissolution and then the samples were cooled to ambient temperature in an unassisted manner. All samples formed crystals that were then isolated by vacuum filtration and air dried; the samples were not washed with solvent.

Optical microscopy and particle sizing

Optical microscopy and particle size measurement were carried out using a Nikon Eclipse 50i polarising microscope with the Nikon Digital Sight DS-Fi1 digital camera and the NIS-Elements software version BR 3.1. A perimeter was established around the visible surface area of individual crystals and the area inside this perimeter was used as the area of the crystal (μm^2). The crystal lengths (μm) were determined by measuring the distance of the longest dimension of visible surface area of each individual crystal.

Powder X-ray diffraction

PXRD was performed at ambient temperature using a Stoe STADI-MP diffractometer operating in transmission mode with a linear PSD detector with an anode current of 40 mA, an accelerating voltage of 40 kV and Cu $K\alpha_1$ radiation (λ = 1.5406 A) scanning in steps of 0.5 ° for 45 seconds per step from 5 to 43 ° in 2θ. Samples were held between acetate foils.

DSC

DSC was carried out on a TGA Q1000 Calorimeter with an RCS 40 cooling system at 2 ºC/min.

Partial dissolutions

Crystals of a similar size within a batch were selected by eye. The samples were subsequently weighed, and the area and length of each individual crystal was determined. The solubility of compound **1** was determined to be 2.94 (±0.05) mg/mL in hexane 18 °C, and so the appropriate amount of solvent was added to dissolve 10 - 20 % of the total particle weight. 2-(2-

Ethylhexyloxy)ethanol was added as a surfactant at a level of 1 μmol per 6 mm^2 of total particle area. Vials containing the sample, surfactant and solvent were stirred using a vortex mixer for 1.5 hours at room temperature at speeds between 300 to 500 RPM depending on volume of solvent within the sample vial. After 1.5 hours the solvent was removed by pipette and placed in a vial to allow the solvent to evaporate and the relative proportion of **1**:additive was determined by HPLC analysis. The partially dissolved crystals remaining in the original sample vial were analysed by microscopy again to determine the length and area of each individual crystal after each dissolution. The partial dissolution procedure was repeated again to dissolve another 10 - 20 % of the total original crystal weight as many times as was necessary with the final dissolution being a complete dissolution of the residual crystals.

Results and Discussion

Impurities may not necessarily be uniformly distributed throughout multi-particle crystal samples, with possible variation of impurity concentration both within and between particles. Methods which allow the determination of the distribution of impurities within batches of particles could guide impurity management in process design. One approach would be to allow for the controlled partial dissolution of multi-particle crystalline samples, such that a reasonably consistent proportion of each particle is dissolved, with analysis of the resulting solutions providing data on composition, and particle sizing showing the particle locations giving rise to that data.

To develop such an approach, it would be preferable to use as the system for study one in which the levels of specific impurities would be both adjustable overall and reasonably evenly distributed throughout. For example, such a system would be provided by the compounds 2-nitro-4-trifluoromethylacetanilide (**1**), 4-methyl-2-nitroacetanilide (**2**) and 4-chloro-2-nitroacetanilide (**3**) (Figure 1), which have been shown to act as isomorphic additives displaying an appreciable degree of mutual lattice incorporation.[32] As the trifluoromethyl group has larger van der Waals radius than the methyl or chloro groups (2.15 Å *vs.* 2.00 Å and 1.80 Å respectively),[37] compound **1** was selected as the main component of the system, i.e. the compound that would ostensibly be crystallised. Compounds **2** and **3** would then act as the impurities, or additives, in crystals of compound **1**, which given their smaller size should be feasible provided the quantities of **2** and **3** are kept low. To provide a comparison to compounds **2** and **3**, compound **4**, which contains the 2-nitro-4-trifluoromethylphenyl core of compound **1** but with the acetamido group replaced by the more sterically demanding pivalamido group,

was selected on the basis that such a compound was less likely to be well incorporated into crystals of **1**.

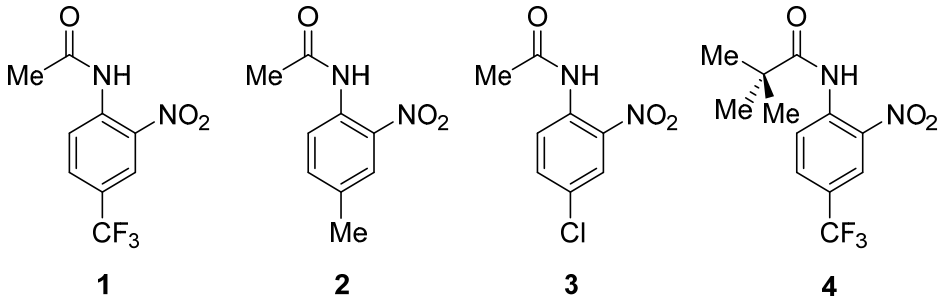


Figure 1. Structures of 2-nitro-4-trifluoromethylacetanilide (**1**), 4-methyl-2-nitroacetanilide (**2**), 4-chloro-2-nitroacetanilide (**3**) and *N*-(2-nitro-4-trifluoromethylphenyl)pivalamide (**4**).

Choice of crystallisation solvent is an important consideration both to achieve useful incorporation of 'impurity' compounds **2**, **3** and **4**, but also to provide crystal particles with morphologies favourable for sequential dissolution. Previous work on compounds **1**, **2** and **3** as isomorphic additives used 50% aqueous ethanol as crystallisation solvent and provided solubility data on these compounds in that solvent.[32] Figure 2 shows the typical morphologies of crystals of compound **1** obtained from a variety of solvents. The crystals obtained from 50% aq. EtOH were found to be fine needles, which would likely be less suitable for sequential dissolution. More suitable prismatic morphologies were obtained from toluene and diethyl ether. As 50% aq. EtOH had been shown to be successful as a crystallisation solvent in which 'mixed' crystals for compounds **1**, **2** and/or **3** could be formed, this solvent was chosen for further study irrespective of the unfavourable morphology of the resulting crystals. Of the solvents giving more prismatic morphologies, toluene was selected as the most practical as a crystallisation solvent. The solubility of compound **1** in 50% aq. EtOH is reported to be 4.98 mg mL^{-1} at 25.5 °C.[35] The solubility of **1** in toluene was found to be 119.0 (±0.4) mg mL^{-1} at 25.0 °C. In 50% aq. EtOH, the solubility of **2** was reported to be 16.50 mg mL^{-1} and that of compound **3** to be 8.52 mg mL^{-1} at 25.5 °C.[35] The solubility of compound **4** in 50% aq. EtOH was found to be 0.47 (±0.05) mg mL^{-1} at 25.0 °C.

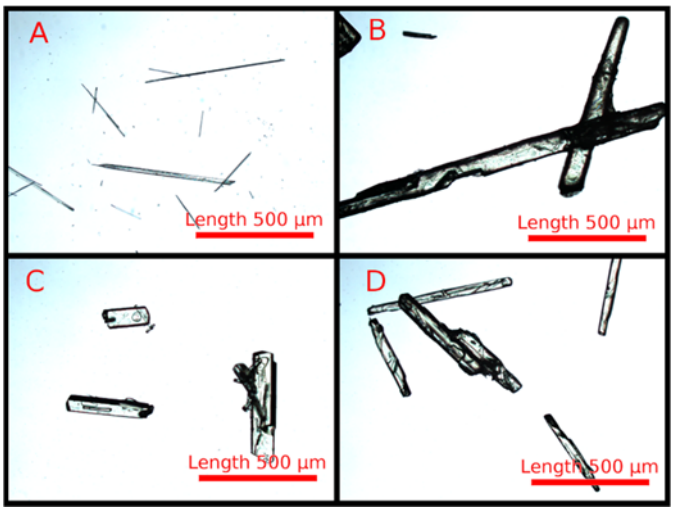


Figure 2. Microscopic images of **1** recrystallised from different solvents displaying various morphologies; (A) 50 % aqueous ethanol, (B) toluene, (C) diethyl ether, (D) dimethylformamide.

Table 1 shows the overall composition of crystals of compound **1** recrystallized from 50% aq. EtOH containing various proportions of compounds **2**, **3** or **4**. The solutions were prepared with a supersaturation (σ) of 2.5 with respect to **1** and levels of compound **2**, **3** or **4** ranging from 1.0 mol % to 10.0 mol %. The trend of incorporation is also shown in Figure 3, showing for each individual additive an ascending pattern, whereby the larger the doping level, the larger the incorporation level. Comparatively, the level of incorporation across every additive series appears to correlate with the solubility of **2**, **3**, and **4**, under the same conditions, the least soluble additive species appears to have a greater incorporation into solid particles of **1** following a trend of **4** > **3** > **2**. The incorporation trend for additives **2** and **3** shown in Figure 3 is consistent, i.e. there is a reasonably linear correlation between the proportion of the additive in solution and the extent of incorporation. For additive **4**, the trend is less consistently linear, with apparently differing behaviour below and above 6.0% proportion in solution.

Table 1. Overall incorporation (% composition by HPLC) of compounds **2**, **3** or **4** in crystals of compound **1** obtained by crystallisation from solutions in 50 % aqueous ethanol containing a quantity of **2**, **3** or **4**, at a σ value of 2.5.

% Additive in solution	% 2 Incorporated	% 3 Incorporated	% 4 Incorporated

1.00	0.216	0.483	0.517
2.00	0.487	0.909	0.887
3.00	0.848	1.263	1.446
4.00	0.980	1.888	1.564
5.00	1.103	2.249	2.106
6.00	1.594	2.792	2.506
7.00	1.760	3.128	3.875
8.00	1.884	4.081	5.292
9.00	2.256	4.744	6.628
10.00	2.600	5.049	7.465

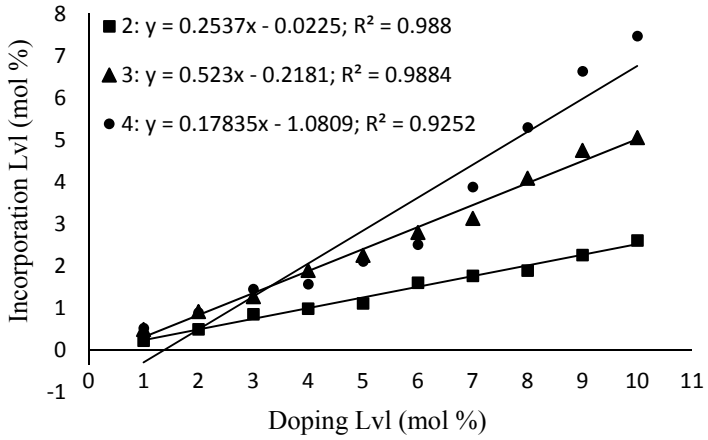


Figure 3. Comparison of the incorporation efficiencies of compound **2**, **3**, or **4** into crystals of compound **1** grown from 50% aq. EtOH at σ = 2.5.

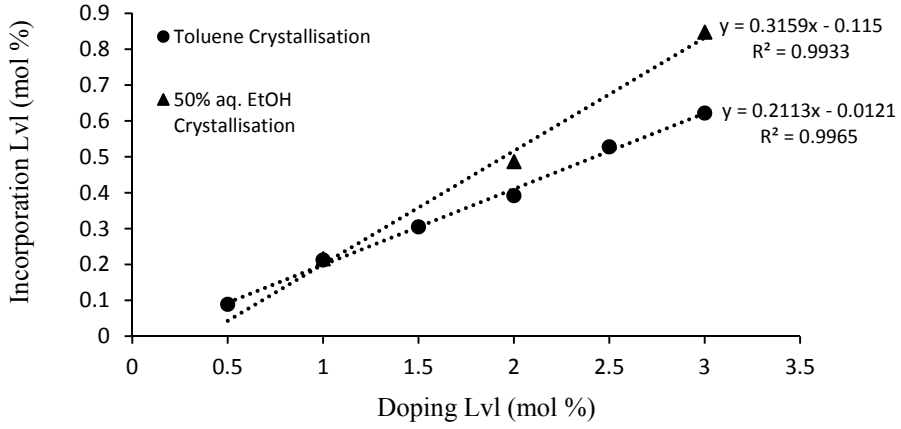
Similar data for toluene as solvent is shown in Table 2. The solutions were prepared with a σ value of 1.5 with additive levels ranging from 0.5 mol % to 3.0 mol %. It can be seen that the trends for incorporation of additives into crystals of compound **1** are different from the series obtained using 50 % aqueous ethanol as a solvent. Compound **2** incorporates into the crystals of **1** at a lower level than **3** (Figure 4a)**.** The incorporation levels of **3** into crystals of compound

1 from toluene solutions produced an additive series with incorporation levels that closely resemble the incorporation levels of **3** in the 50 % aqueous ethanol series (Figure 4b). Compound **4**, which in the 50% aq. EtOH series was overall the most highly incorporated additive, has the lowest level of incorporation using toluene as a solvent (Figure 4c). Concentrations of additive **4** are below the limit of detection at a doping level of 0.5 mol %. The affinity of **4** over **1** for non-polar media has been observed from thin-layer chromatography on silica gel [R_f(**4**) = 0.55; Rf(**1**) = 0.17 in 1:7 EtOAc:hexane] and reverse-phase high performance liquid chromatography [t_R(**4**) = 23.275 mins; t_R(**1**) = 12.726 mins], inferring that the solubility of **4** should be higher than the solubility of **1** in toluene, such that relatively little of the **4** solvated species is incorporated into the crystallising **1** structure. Toluene was selected as the better solvent system for growing crystals of compound **1** with favourable morphology for stepwise partial dissolution containing quantities of additives **2** or **3** as impurities, while 50% aq. ethanol was used for examining incorporation of additive **4**.

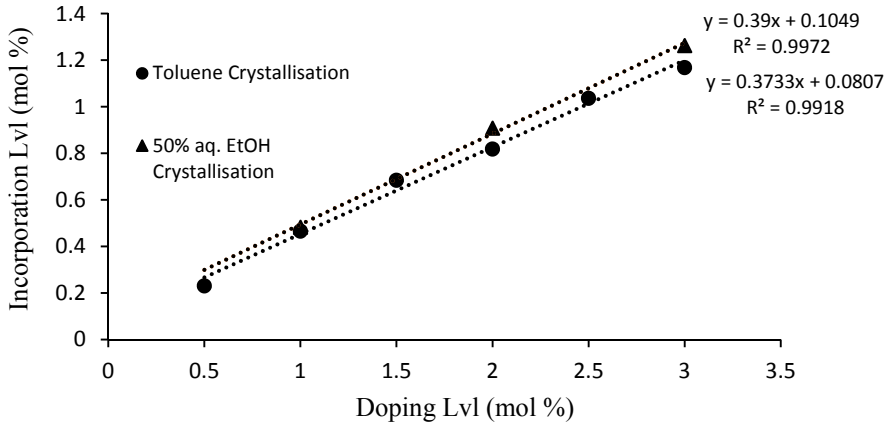
Table 2. Overall incorporation (% composition by HPLC) of compounds **2**, **3** or **4** in crystals of compound **1** obtained by crystallisation from solutions from toluene containing various quantities of **2**, **3** or **4**, at a σ value of 1.5.

% Additive in solution	% 2 Incorporated	% 3 Incorporated	% 4 Incorporated
0.5	0.089	0.231	Undetected
1.0	0.212	0.466	0.018
1.5	0.305	0.685	0.023
2.0	0.391	0.818	0.055
2.5	0.527	1.036	0.057
3.0	0.622	1.168	0.065

(a)



(b)



(c)

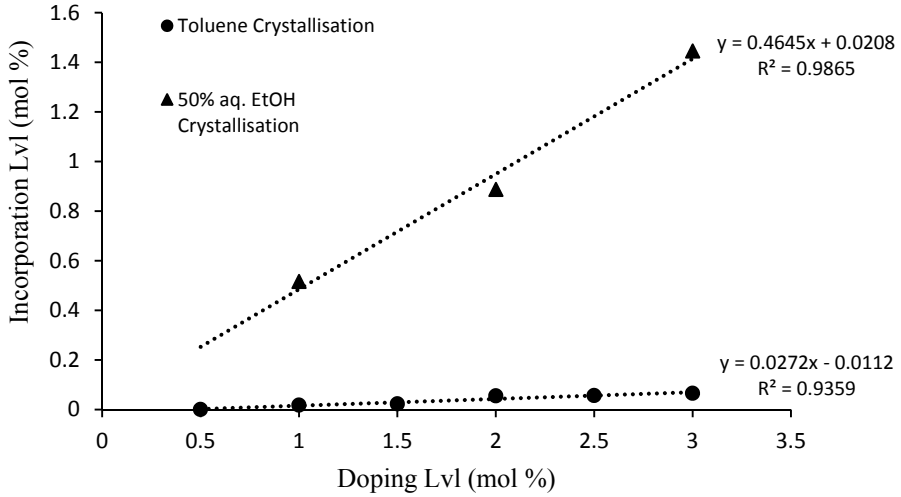


Figure 4. Comparison of the incorporation efficiency of **(a)** additive **2**, **(b)** additive **3** and **(c)** additive **4** into crystals of compound **1** grown from toluene and 50 % aqueous ethanol.

Figure 5 shows the PXRD pattern for **1** grown in toluene at σ = 1.5 against the PXRD patterns for **1** grown in 50 % aqueous ethanol at σ = 2.5 with 10 mol % additions of **4**, **3**, and **2**. PXRD patterns were obtained for crystals of **1** with additive concentrations as low as 1 mol % grown under the aforementioned conditions. For samples containing additive **3** or **2** there was no discernible formation of additional peaks up to the highest concentration of 10 mol %. All obtained patterns displayed peaks corresponding to pure **1** with only minor differences in the intensities of several peaks. Similar to the patterns obtained for crystals containing additives **3** and **2**, the patterns for **4**-doped **1** samples resemble the pattern for pure compound **1**. Between the doping levels of 6 mol % and 10 mol % an additional peak can be observed at ~21 ° 2θ. This additional peak corresponds to the second most intense peak observed in the PXRD spectrum of pure **4**, the most intense peak appears at ~8 ° 2θ in the pure compound and so it may be overlapping with a similarly positioned peak of **1** in the additive series. This indicates that separate particles of compound **4** may be forming from aq. EtOH solutions containing 6 mol % and greater levels of additive **4**. It should also be noted that the doping levels in the range of 6 mol % to 10 mol % also produced deviations in the trend for incorporation of additive **4** into crystals of compound **1** as seen in Figure 3. The relatively non-linearity in the degree of incorporation of additive **4** relative to the proportion in solution may be associated with the formation of separate particles of compound **4** from 50% aq. EtOH solution containing over 6% of that compound. Figure 6 shows the PXRD pattern for **1** grown in toluene at σ = 1.5 against the PXRD patterns for **1** grown in toluene at σ = 1.5 with 3 mol % additions of **3** and **2**. PXRD patterns were obtained for crystals of **1** with additive concentrations as low as 0.5 % grown under the aforementioned conditions. For samples containing **3** or **2** there was no discernible formation of additional diffraction peaks up to the highest concentration of 3 mol %. All obtained patterns displayed peaks corresponding to pure **1** with only minor differences in the intensities of some peaks. Examples of DSC data for samples containing additives **3** and **2** can be seen in Figures 7 and 8. The inclusion of these additives lowers the melting point of the crystals compared to that of pure compound **1** with the larger the amount of additive present, the further the melting point shifts towards the melting point of pure **2** or **3**. No secondary events such as polymorph changes or minor melting point events were observed under these conditions. Samples incorporating additive **4** displayed similar trends of the melting point gravitating towards that of **4** from **1** with each increasing doping concentration; however, when the doping level is at 6 mol % and upwards, the emergence of an endothermic event begins to appear at approximately 70 °C (Figure 9). This minor thermal event occurs at a lower

temperature than the melting points of either **4** or **1**, determined by DSC to be 91.96 °C and 112.06 °C respectively. The TGA curve for 8 mol % **4**-doped **1** is overlaid with the DSC curve for the same sample (Figure S4) shows no weight loss occurring around the 70 °C thermal event.

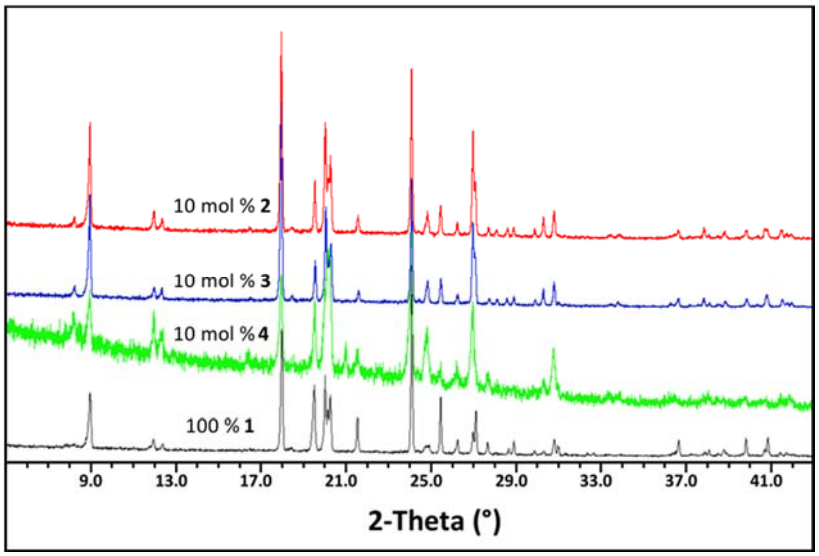


Figure 5. Powder X-ray diffraction patterns obtained for crystals of **1** (black), **1** grown from 50 % aqueous ethanol with concentrations of 10 mol % **4** (green), 10 mol % **3** (blue), and 10 mol % **2** (red).

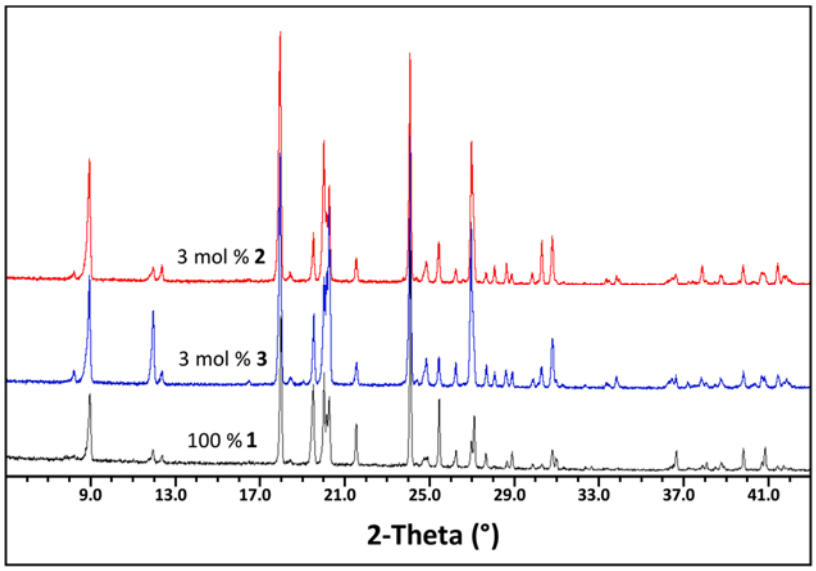


Figure 6. Powder X-ray diffraction patterns obtained for crystals of **1** (black), **1** grown from toluene with concentrations of 3 mol % **3** (blue), and 3 mol % **2** (red).

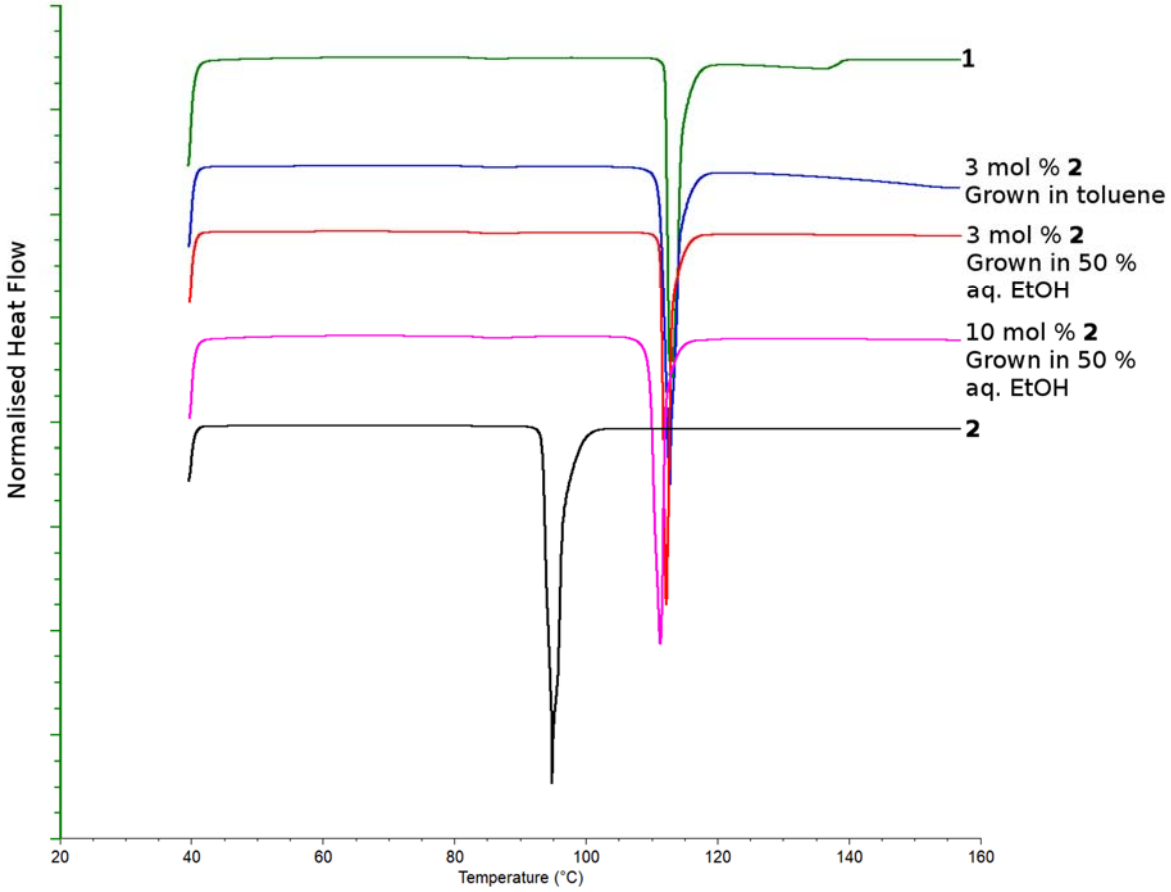


Figure 7. Examples of DSC curves obtained from crystals of **1** containing varying amounts of additive **2**.

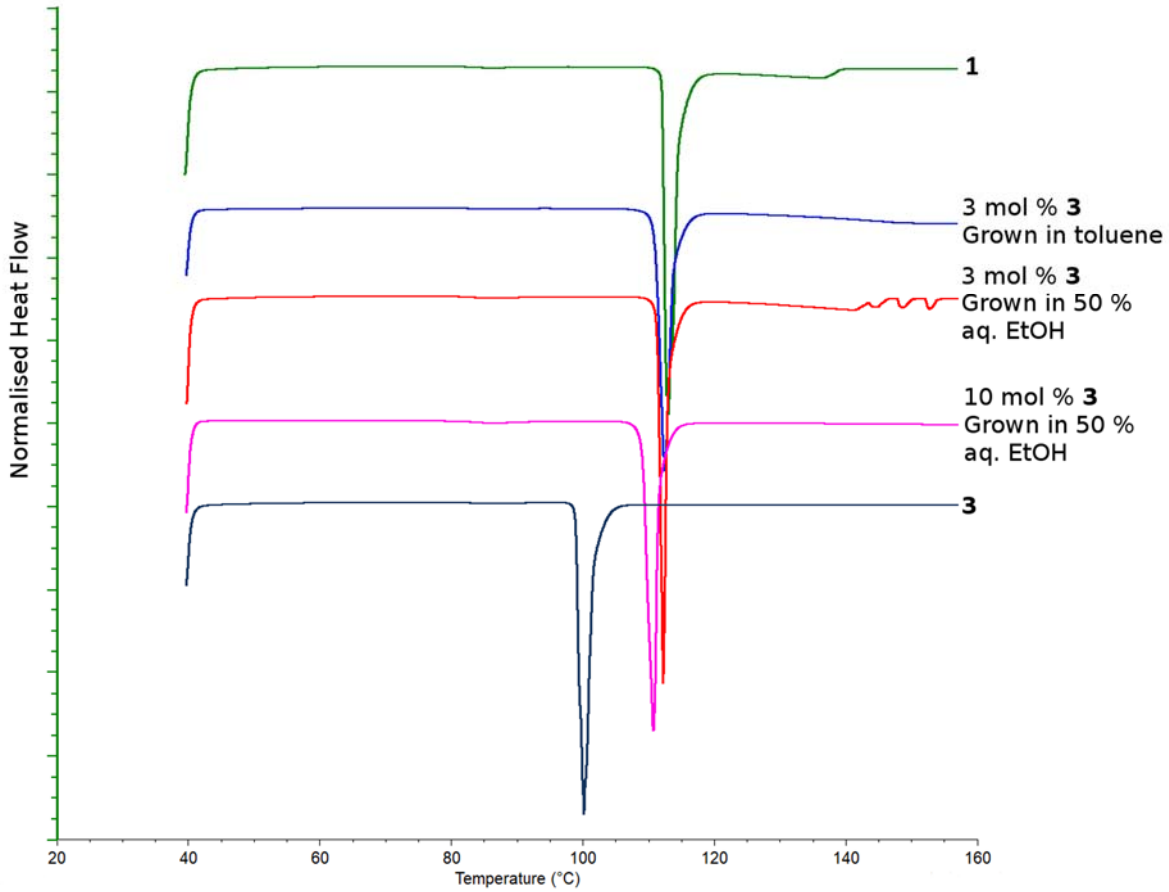


Figure 8. Examples of DSC curves obtained from crystals of **1** containing varying amounts of **3**.

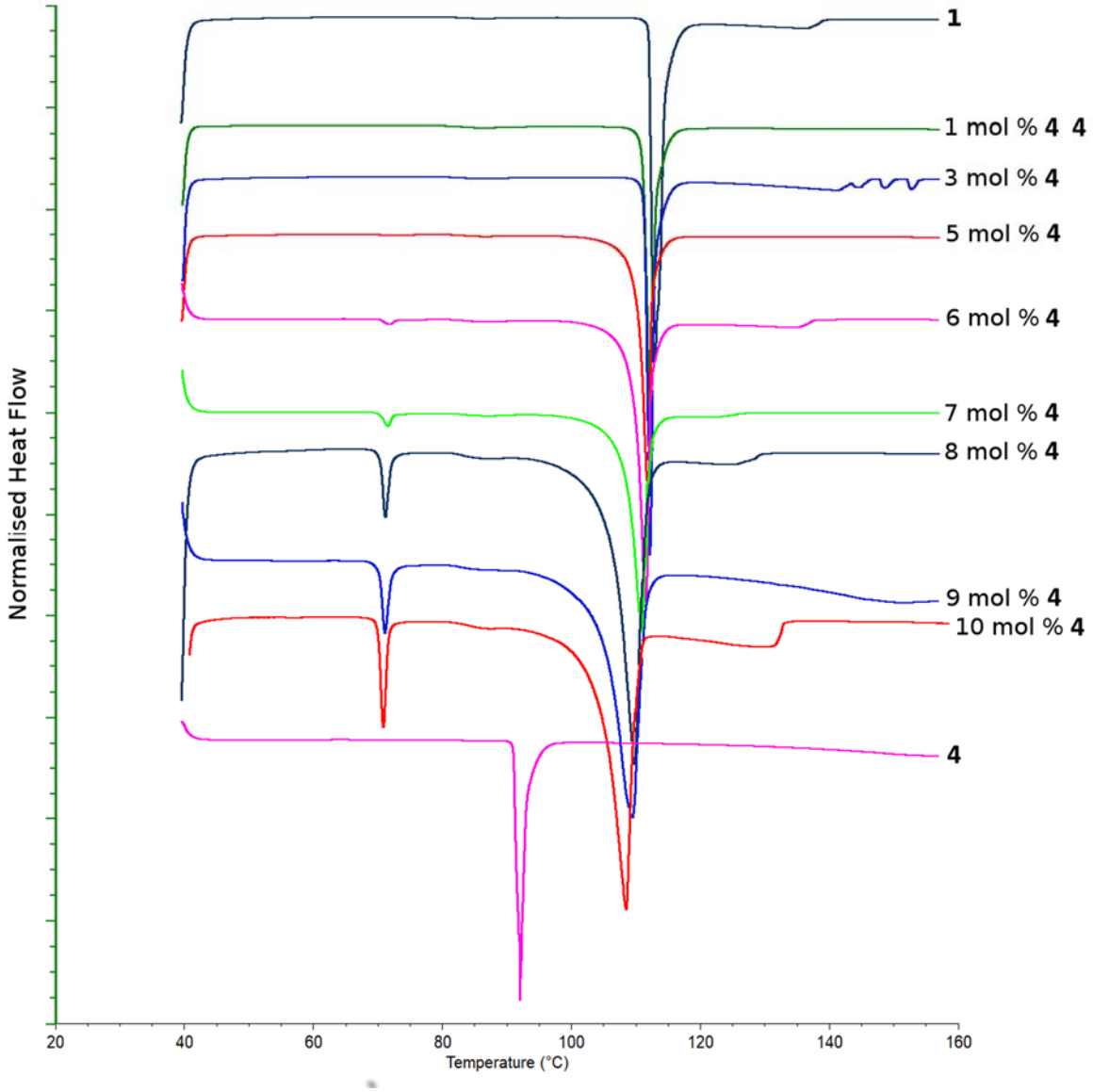


Figure 9. DSC curves obtained from crystals of **1** containing varying amounts of **4**.

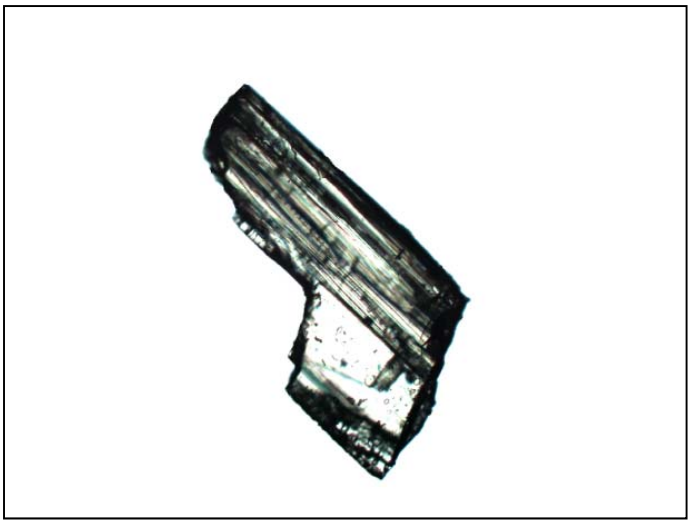
The aim of the present study is to analyse the composition of multi-particle solids in such a way that the composition data obtained can be assigned to reasonably defined locations in the sample of particles. Work on compounds **1**, **2** and **3** as isomorphic additives used HPLC to determine the degree of additive inclusion, and confirmed the homogeneity of inclusion by subjecting material placed on a fritted funnel to serial washes until fully dissolved, with HPLC analysis of the solutions from each wash.[32] In preliminary work in our studies, stepwise dissolution of material supported on a sintered glass funnel was investigated. However, examination of particles before and after washing found that extensive fusing of particles to give larger aggregates had occurred, so that such an approach was not suitable for our work.

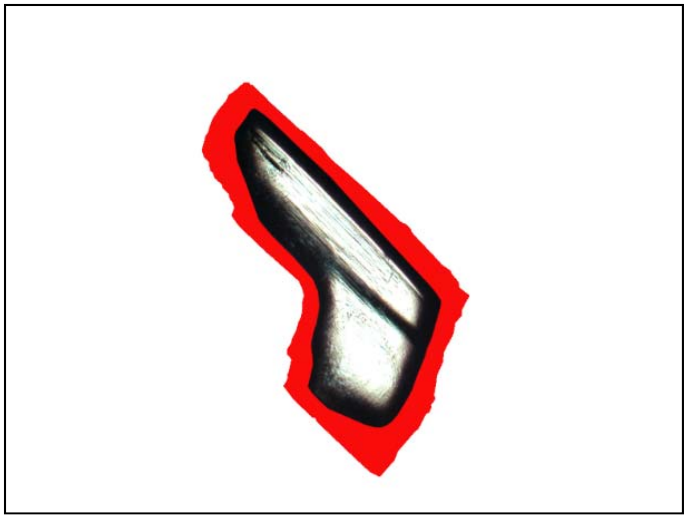
Instead, we opted to develop a dissolution medium approach. This was to be achieved by dissolving a relatively consistent amount of each particle, analysing the resulting solution for composition data, and using before-and-after particle sizing to identify the locations to which that data can be assigned. Doing this required that *(i)* the particle be inhibited from aggregating or flocculating, i.e. that the integrities of the individual particles be conserved as much as possible, and *(ii)* that a reasonably controlled or predictable portion of each particle be dissolved. Inhibition of the flocculation of particles in suspension has been extensively studied as an aspect of colloid science.[38,39,40] Dissolution has also been extensively studied, especially in the context of dissolution of pharmaceutical particles in the gastrointestinal tract, and models capturing the various parameters involved devised, such as the Noyes-Whitney / Nernst-Brunner equations.[41,42]

Inhibition of flocculation is generally achieved by the use of surfactants and polymers which lower solid-liquid interfacial tension and provide steric stabilisation. Non-ionic surfactants have been used for this purpose.[43] For the purposes of the present study, a non-aqueous non-polar continuous phase was the preferred vehicle for ease of isolation of organic compounds for analysis, therefore a non-ionic surfactant would be preferred. However, in this initial study, a high molecular weight surfactant was felt to be undesirable due to possible impact on extraction of compounds for analysis. 2-(2-Ethylhexyloxy)ethanol was selected as a moderate molecular weight compound which retained the essential features of a non-ionic surfactant. This compound has been used in cosmetic formulations and has a HLB (hydrophilic-lipophilic balance) value of approximately 7.5, similar to that of higher molecular weight emulsifying agents.[44] Studies on the use of 2-(2-ethylhexyloxy)ethanol in the systems described herein found 1 μmol per 6 mm^2 particle surface area to be adequate for anti-flocculant activity.

In the Noyes-Whitney / Nernst-Brunner model, the driving force for dissolution is the difference in concentration in the bulk dissolution medium and the saturation concentration in that medium under those conditions.[41,42] For the purpose of the present study, a medium was required which would act as a liquid vehicle for the particles and also act as a moderate to weak dissolution medium. 2-Nitro-4-trifluoromethylacetanilide (**1**) was found to be weakly soluble in hexane [2.94 (±0.05) mg mL^{-1} at 18 °C; cf. 119.0 (±0.4) mg mL^{-1} in toluene at 25 °C], hence that solvent was selected. To demonstrate the concept of controlled partial dissolution of multi-particle batches, a sample of 50 crystals of compound **1** was suspended in hexane containing 1 μmol of 2-(2-ethylhexyloxy)ethanol per 6 mm^2 particle surface area. The size (length and surface area) of crystals were determined by optical microscopy image analysis (Figure 10).

The volume of hexane was selected to allow for ca. 10 - 20% dissolution. After agitation for 1.5 h, the crystals were sized. The crystals were subjected to further such dissolution steps. The data obtained, shown in Figure 11, suggests that the concept of controlled partial dissolution of multi-particle samples is feasible. In particular, it should be noted that the number of crystals remained constant, and that while the size of the crystals decreased with each dissolution step as required, the overall spread of the size distributions was reasonably conserved. The D10, D50 and D90 values for the four distributions shown in Figure 11 are listed in Table 3.





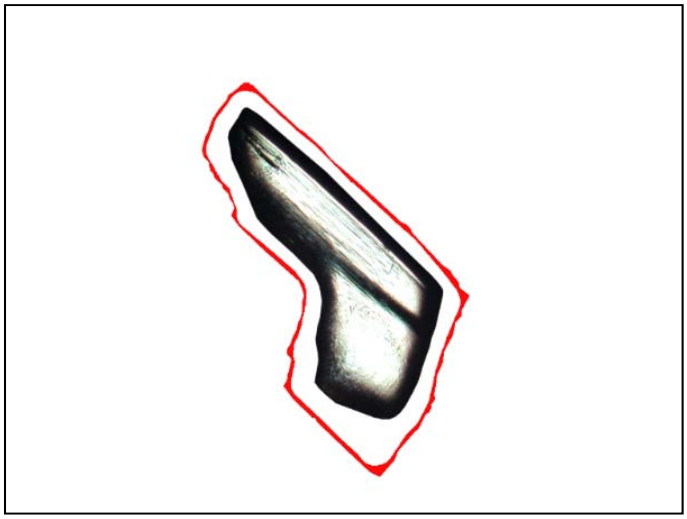


Figure 10. Partial dissolution and analysis of crystals of compound **1**; (top) initial crystal sized by microscopy, (centre) area in red dissolved for analysis by HPLC, (bottom) residual crystal sized by microscopy.

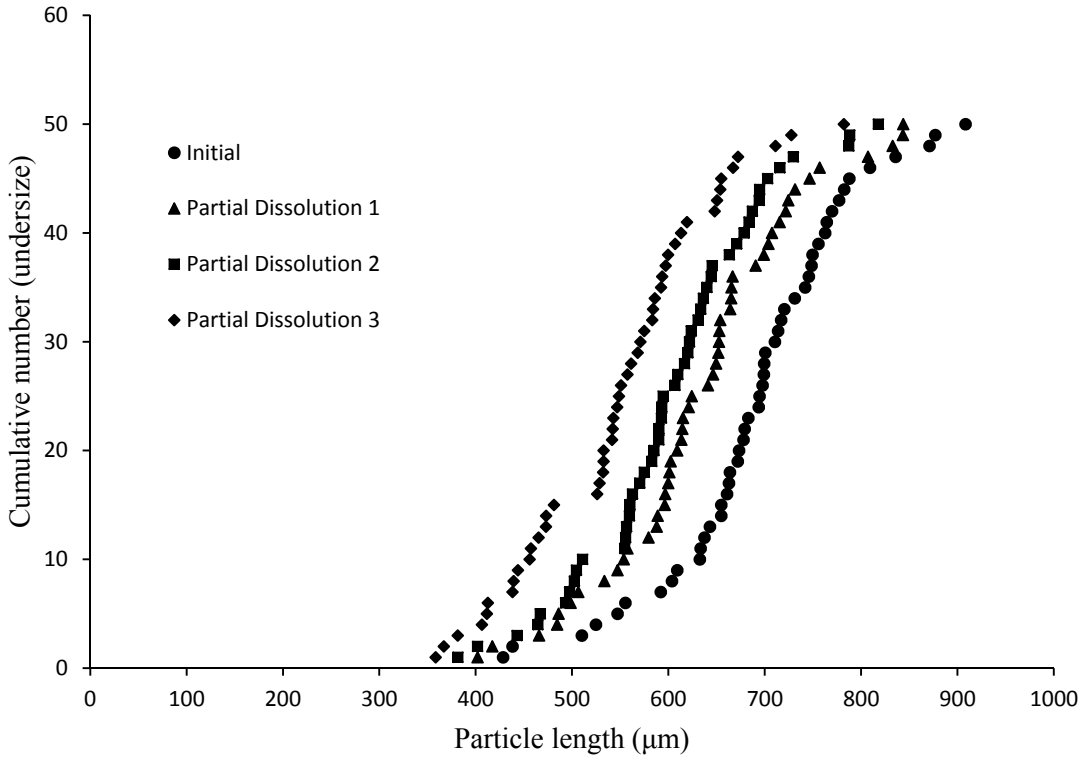


Figure 11. Data on the stepwise dissolution of a sample of 50 crystals of compound **1**.

Table 3. D10, D50 and D90 values obtained from the data on the stepwise partial dissolution (PD) of a sample of 50 crystals of compound **1**.

Measurement	Initial	PD1	PD2	PD3
Length D_{10} (μm)	547.08	486.03	467.12	411.52
Length D_{50} (μm)	694.48	624.19	594.63	548.69
Length D_{90} (μm)	787.69	746.44	702.89	654.77
Area D_{10} (μm^2)	71603.73	52336.15	49063.59	42799.48
Area D_{50} (μm^2)	122672.5	97019.31	89171.01	70324.44
Area D_{90} (μm^2)	190622.8	166361.8	136154.5	115749.8

To facilitate analysis of the composition of crystals based on sequential dissolution, samples of eight or twelve similarly sized crystals of 2-nitro-4-trifluoromethylacetanilide **1** which had been grown from a solution containing quantities of added impurity **2**, **3**, or **4** as described above were selected. On a larger scale, this would correspond to selection of a size classified group based on, for example, sieving. The area and length of the crystals were measured by optical microscopic image analysis as described above before and after dissolution steps. The crystals were suspended in sufficient hexane to provide for dissolution of ca. 10% of each particle based on the solubility of **1** in hexane determined above. 2-(2-Ethylhexyloxy)ethanol was added to inhibit flocculation, as described above. The samples prepared in this manner were agitated for 1.5 hours after which the composition of the resulting solutions were analysed by HPLC and the particles again size analysed. Examples of the series of crystal size distributions obtained by this process are shown in Figure 12 and Figures S5-S26. These show the diminishing sizes of the crystals consequent upon each dissolution step. On some occasions, two successive distributions 'crossed-over' to some extent, e.g. as in Figure S8. The degree of dissolution is generally not perfectly uniform for each crystal in any batch, which is a reasonably common finding in the dissolution of batches.[45] However, at least for these small trial samples, the individual crystals could be dissolved to a reasonably controllable extent, providing solutions for analysis.

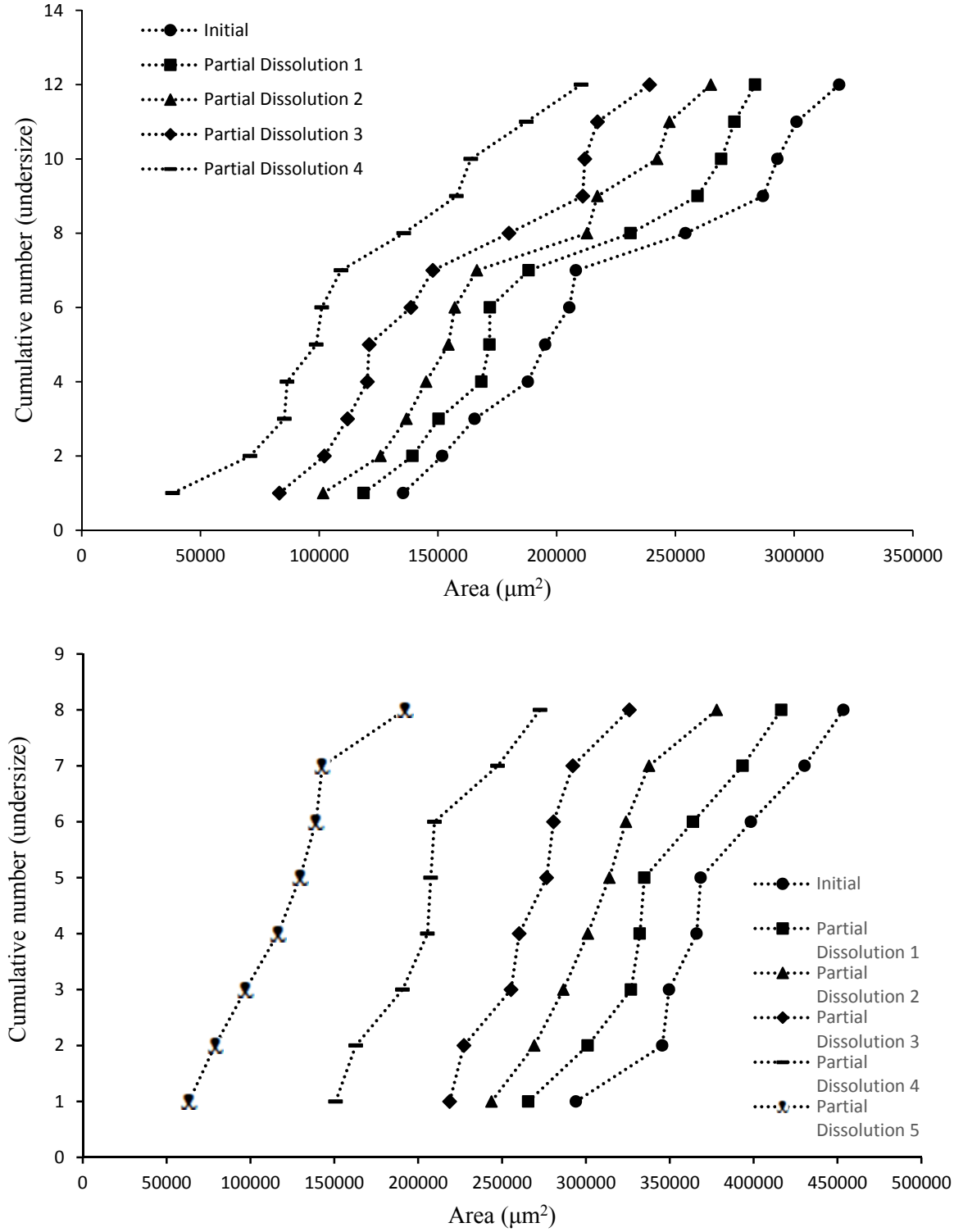


Figure 12. (top) Series of crystal size (by area) distributions obtained from twelve crystals of compound **1** grown from solutions containing 1.5 mol % of additive **2**; (bottom) series of crystal size (by area) distributions obtained from eight crystals of compound **1** grown from solutions containing 2.5 mol % of additive **3**.

The solutions obtained after each dissolution step were subjected to analysis by HPLC allowing the proportion of the additive in that solution to be determined. This value could be assigned to regions of the crystals as follows. Each measurement of the level of additive was assigned to a dissolution mid-point, based on the mean size of the series of crystals before and after each dissolution step. The crystals were sized by length and area. Area values were used in the data processing described herein as the area measurement is less dependent on morphology and choice of diameter than length measurement. The mean sizes are then expressed as percentages remaining of the initial mean size, giving the percentage dissolved, i.e. 0% dissolved of the initial particles, 100% dissolved when no particles remain. The dissolution mid-point is then the percentage defined in this way at the percentage prior to a dissolution stage plus half difference in values before and after the dissolution stage. Plots of the levels of additive *vs*. dissolution mid-point as so defined are shown in Figure 13 for the series of dissolutions shown in Figure 12. Corresponding plots for the other dissolution series studies are shown in Figures S27 to S36.

All of these plots show that the distribution of added impurities **2** and **3** in samples of crystals of compound **1** is relatively even throughout. Given that compounds **1**, **2** and **3** have been shown to behave as isomorphic additives with capability for incorporation into crystal lattices by mutual substitution, this finding is not surprising.[32] In fact, compounds **1**, **2** and **3** were selected for this study because it was known that they would exhibit such behaviour. A contrasting example of an added impurity not behaving in this way, i.e. compound **4**, is described below. However, the approach described herein has determined this distribution of impurities **2** and **3** in crystals of compound **1** independently by controlled sequential dissolution of samples of multiple crystals, in conjunction with accompanying composition and size analysis.

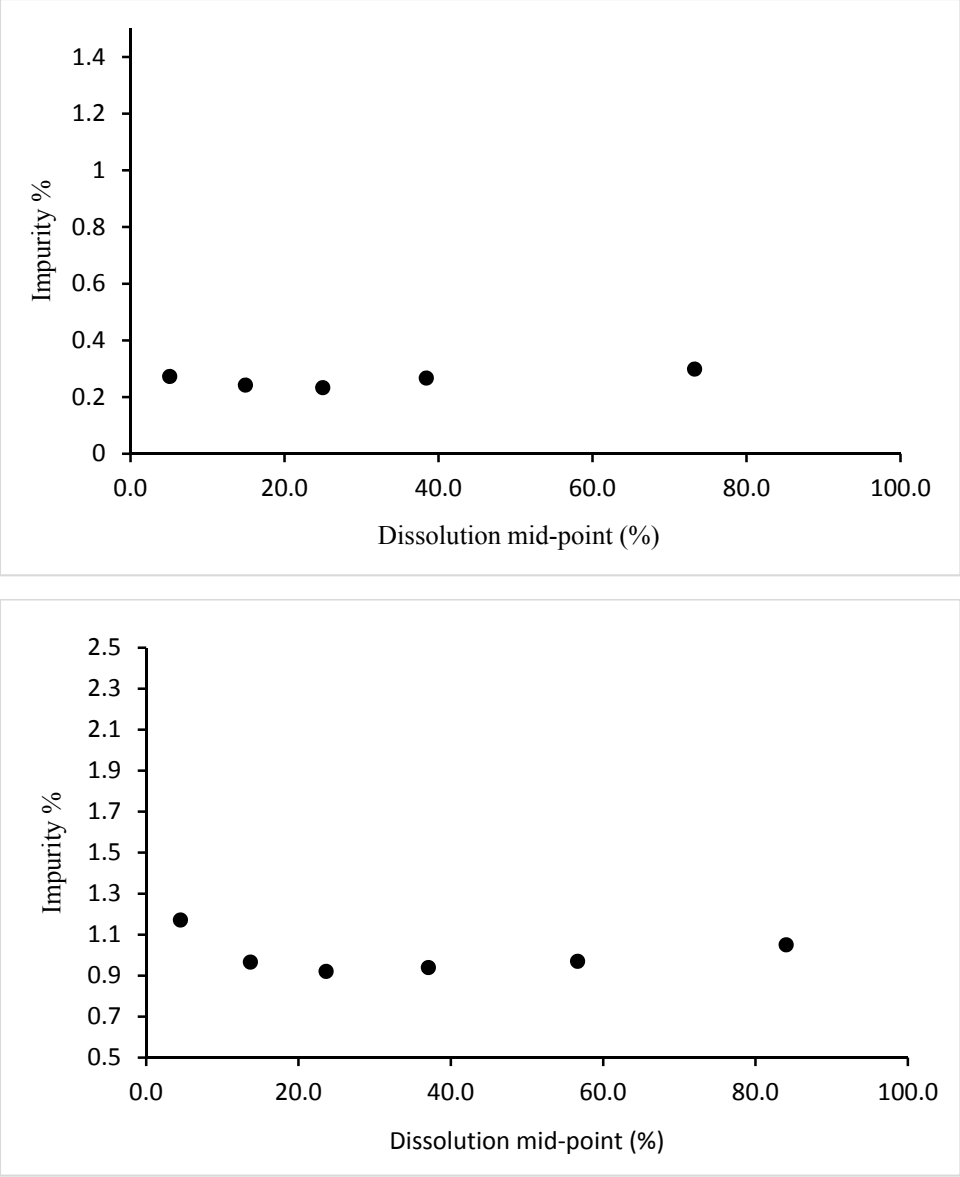


Figure 13. Plot of percentage by HPLC of added impurity in crystals of compound **1** *vs.* the dissolution mid-point for the sample as defined in the text; (top) of crystal grown from solutions containing 1.5 mol % of additive **2**; (bottom) of crystals grown from solutions containing 2.5 mol % of additive **3**.

The distributions shown in Figures 13 and Figure S27 to S36 are not perfectly uniform but show some variation, ranging from relative standard deviations of less than 10% to ca. 13% (e.g. Figure S29) to ca. 17.5% (e.g. Figure S30) up to 24.5% (e.g. Figure S28). These variations arise from both the imprecisions of the method and also the likelihood that the added impurities are not replacing molecules of compound **1** in the crystal lattice with perfect regularity. In many

cases (e.g. Figure 13b), the highest level is found in the first dissolution steps and the lowest levels in second or third steps, with an increase in level towards the final dissolution steps. As this pattern is not observed in all cases, it is not possible to say definitively whether it is a systematic consequence of the methodology, although it may be. The higher impurity levels in the first, outermost, dissolution may be due to evaporation of solvents from additive-enriched solution residues on the crystals surfaces. Variations in the relative quantities of additives to crystallising compound remaining in solution during crystal growth may also be involved. The crystals used in the stepwise dissolutions were selected from larger samples. Comparisons of the average impurities levels in the stepwise dissolution, weighted by the proportion dissolved in each step, with the impurities levels measured for the parent batches are shown Table 4. In some cases these correspond closely, e.g. for crystals grown from solutions containing 1.5% of additive **2**, these values differ by only 0.001% (entry 3), but most show a degree of divergence with the weighted average usually being lower, e.g. the values for crystals grown from solution containing 2.0% of additive **3** differ by 0.106% (entry 10). This may reflect a bias due to the selection of similarly sized crystals.

Table 4. Comparisons of parent batch average and weighted averages from stepwise dissolutions.

Entry	Additive	% Additive in soln.	% Additive in parent sample	Weighted % additive in dissolution sample*	Difference (%)
1	2	0.5	0.087	0.088	-0.001
2	2	1.0	0.208	0.185	+0.023
3	2	1.5	0.299	0.268	+0.001
4	2	2.0	0.384	0.370	+0.014
5	2	2.5	0.518	0.440	+0.078
6	2	3.0	0.611	0.539	+0.072
7	3	0.5	0.221	0.191	+0.030
8	3	1.0	0.466	0.405	+0.061
9	3	1.5	0.685	0.601	+0.084
10	3	2.0	0.783	0.677	+0.106
11	3	2.5	0.992	1.002	-0.010
12	3	3.0	1.118	1.204	-0.086

*The weighted average was determined from the HPLC data using the following formula:

$$\sum_{i=1}^{n}\left(\frac{D_i}{\sum_{i=1}^{n} D_i}\right)\cdot R_i$$

where n is the number of partial dissolutions in a dissolution series, D_i is the number of moles dissolved in a partial dissolution step i, and R_i is the percentage of additive in the solution obtained from partial dissolution step i.

Assuming the crystals can be approximated as homogenous solid solutions, Berthelot-Nernst's law can be applied to give the distribution coefficient, α, in terms of the mole fractions of the impurity in the solid and liquid phases, i.e. X_{imp}^{S} and X_{imp}^{L} respectively.[46]

$$\alpha = \frac{X_{imp}^{L}\left(1 - X_{imp}^{S}\right)}{X_{imp}^{S}\left(1 - X_{imp}^{L}\right)}$$

Table 5 shows the variation of the distribution coefficients calculated from data obtained from each of the dissolution steps for the crystals of compound **1** obtained from solutions containing 1.5% of additive **2** and 2.5% of additive **3**. These data indicate that under these specific conditions, purer crystals of compound **1** are obtained from the solutions containing 1.5% of additive **2** rather than from those containing 2.5% of additive **3**. More interestingly, comparison of the distribution coefficients between dissolution steps show that while they remain within a narrow range, some variation is observed, suggesting that the material precipitating on the crystal surfaces is not perfectly uniform during the crystal growth process.

Table 5. Distribution coefficients, α, determined from data obtained from each dissolution steps on crystals of compound **1** obtained from solutions containing 1.5% of additive **2** and solutions containing 2.5% of additive **3**.

Entry	1.5% (**2**) Dissolution mid-point (%)	α	2.5% (**3**) Dissolution mid-point (%)	α
1	5.1	5.58	4.5	2.16
2	14.9	6.28	13.7	2.63
3	25.0	6.52	23.6	2.76
4	38.4	5.69	37.1	2.71
5	73.3	5.09	56.7	2.62
6	-	-	84.1	2.42

The spread of the degree of dissolution of the series of crystals can be shown using the standard deviations of the extents of dissolution. For example, Figure 14 shows again the data from a series of crystals obtained from solutions containing 2.5% of additive **3**, but with the addition of error bars representing the standard deviations of the series of crystals; allowing for the data processing required to obtain the dissolution mid-points, i.e. the error bars are equal to the square roots of the sum of the appropriate standard deviations squared. This representation shows the variation in the concentration of the impurity as a function of the dissolution region of the crystals, as in Figure 13 above, but also the spread of widths of these dissolution regions within the samples of crystals.

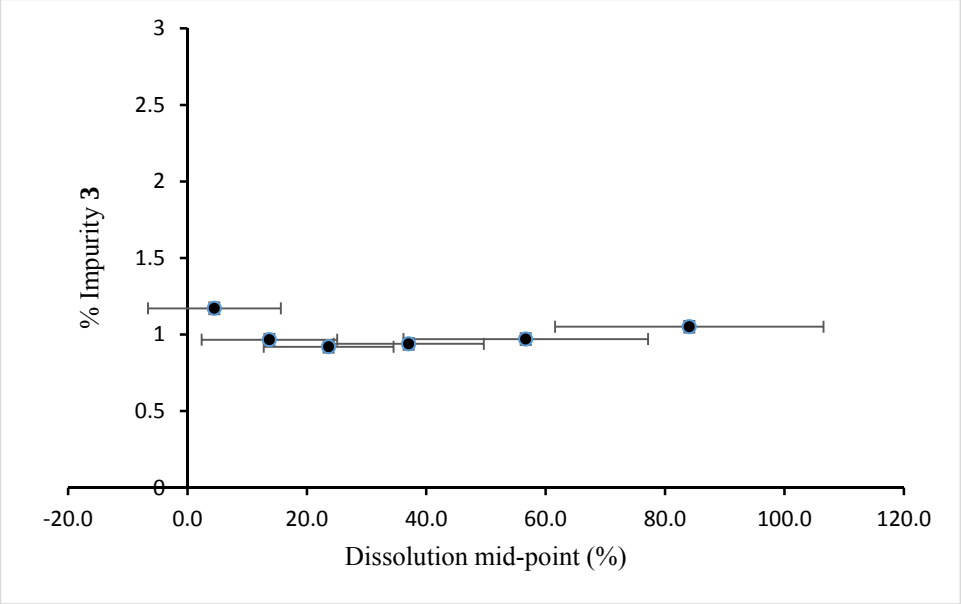


Figure 14. Plot of percentage by HPLC of added impurity in crystals of compound **1** *vs.* the dissolution mid-point for the sample of crystal grown from solutions containing 2.5 mol % of additive **3**, with the addition of bars showing the standard deviation in the extents of dissolution of the crystals.

As noted previously, the methodology described above is an extension to multi-particle samples of previous work on stepwise dissolution on large single crystals.[4,34] For comparison and to provide a better understanding of the stepwise dissolution process, particularly of the later dissolution steps, a series of dissolutions was also carried out on a single large crystal of compound **1** with an area of 958099.0 μm^2 grown from a solution containing 3.0% of added impurity **3**. This crystals was subjected to a series of 12 finely controlled dissolutions. Figure 15 shows images of this crystal after the later stepwise dissolution stages. The images show that the dissolution steps are not precise de-layering processes but instead remove mass in an irregular manner which results in an uneven surface and outline, and pore formation. This adds a degree of imprecision to the location of the removed mass to a particular region of the crystal. Nonetheless, the reduction of crystal mass by sequential stepwise dissolution is controllable and graduated within these limits. The dissolution *vs*. composition data for this crystal is shown in Figure S37. This shows the highest level of impurity **3** (1.8%) in the first dissolution stage, possibly reflecting additional material adhering from surface evaporation of residual solvent, with an average 1.1% of impurity in the subsequent stages.

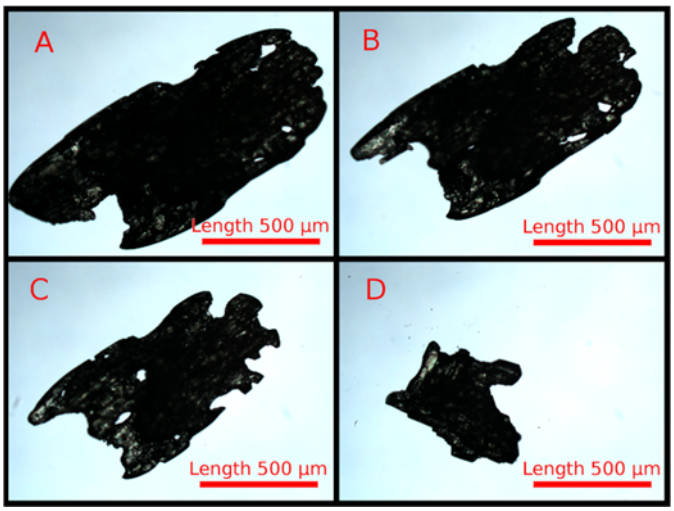


Figure 15. Microscope images of a single crystal of compound **1** grown from solution containing 3.0% of additive **3**, having been subjected to a series of partial dissolution steps. The images depict the crystal after the (A) 9th, (B) 10th, (C) 11th, and (D) 12th dissolution.

As noted above, the uptake of pivalamido additive **4** into crystals of compound **1** grown from toluene was very low, whereas the incorporation of **4** from crystals grown from 50% aq. ethanol was quite high (Figure 4(c)). Hence, crystals grown from 50% aq. ethanol were used to study the distribution of additive **4**. However, as shown in Figure 2, when grown from 50% aq. ethanol, compound **1** forms very fine needles that were not suitable for manipulation necessary for imaging by optical microscopy. Hence, for the series of stepwise dissolutions of crystals containing additive **4**, the crystals were not individually sized by microscope image analysis, but instead the mass dissolved in each dissolution step was determined, in conjunction with HPLC analysis of the resulting solution. This is clearly less satisfactory than the approach taken for additives **2** and **3**, but nonetheless provides some data illustrative of the disposition of compound **4**.

The data obtained in this manner is summarised in Figure 16. For the crystals grown from solutions with low concentrations of additive **4** (0.5% and 1.0%), a low level of additive (ca. 0.2%) was found in every dissolution step. Crystals grown from solutions containing greater than 1.0% of additive **4** showed the highest concentration of additive **4** in the first dissolution step and generally lesser concentrations in each successive dissolution step. This is most striking in the case of crystals grown from solutions containing 3.0% of additive **4**. For these crystals, the first dissolution layer contained 3.5% additive **4**, and the level of additive **4** decreased successively with each step to give 0.4% in the final measurement. By comparison,

data for crystals obtained from solutions containing 3.0% of additives **2** or **3** (Figures S31 and S36) had maximum and minimum levels of 0.64% and 0.44% for additive **2** and 1.46% and 1.09% respectively for additive **3**. The data for additives **2** and **3** was obtained using sizing of individual crystals before and after dissolutions. Nonetheless, the wider range of levels of additive **4**, decreasing with increasing degree of dissolution, i.e. corresponding to greater depth within crystals, is consistent with the increased steric demand of the pivalamido group of **4** compared to the acetamido group of **1**, and the consequent lesser potential to act as an isosteric lattice replacement molecule in crystals of compound **1**.

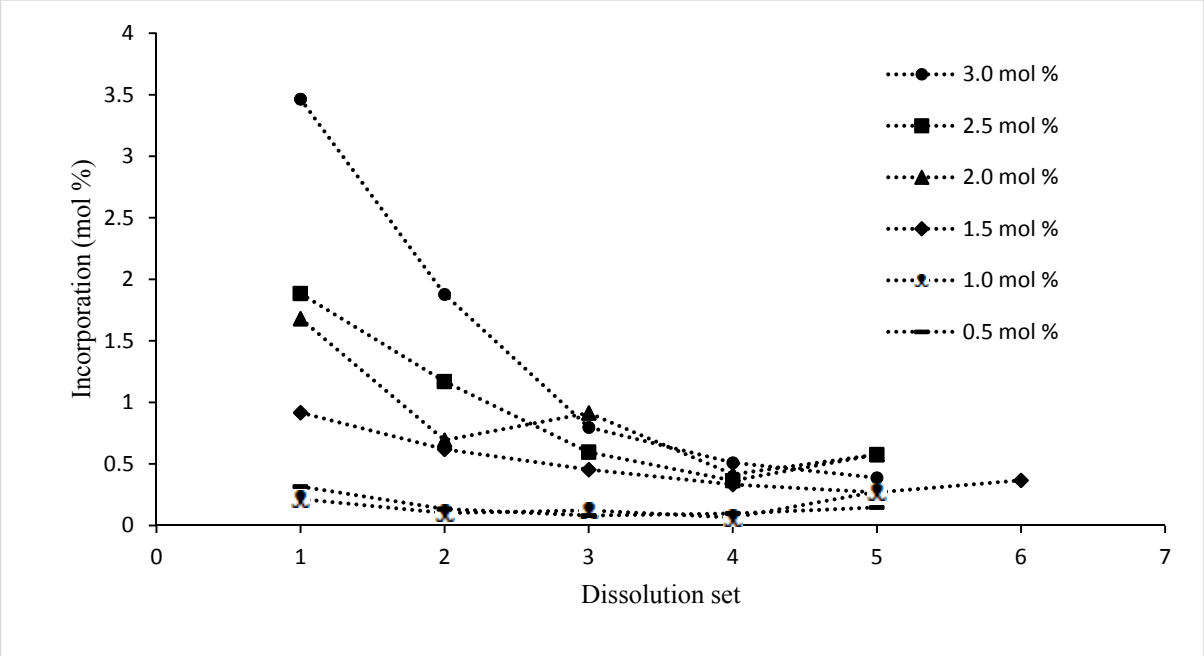


Figure 16. Concentrations of additive **4** in solution obtained by stepwise dissolution of crystals of compound **1** grown from 50% aq. EtOH solutions containing up to 3.0% of additive **4**.

The overall findings described above, that additives 4-methyl-2-nitroacetanilide (**2**) and 4-chloro-2-nitroacetanilide (**3**) are relatively evenly distributed within particles of 2-nitro-4-trifluoromethylacetanilide (**1**) [and that by comparison *N*-(2-nitro-4-trifluoromethylphenyl)pivalamide (**4**) is not evenly distributed] are not at all surprising in that the system of compounds **1**, **2** and **3** was specifically selected on the basis that compounds **2** and **3** would be known to substitute for molecules of compound **1** in a relatively evenly distributed manner.[32] That the controlled sequential dissolution method described herein confirms this distribution, both in terms of the percentage of additives incorporated and the

even distribution of incorporation, is evidence that the method has value for providing such data in cases where the distribution is not known.

In principle, this approach should be highly applicable to multi-particle samples produced in process chemistry development and support. The approach is compatible with widely used methods for composition and size analysis. The information provided can distinguish between different modes of impurity occurrence, such as impurities present largely on the surfaces or near the surfaces of particles, impurities which are incorporated throughout particles but not in an even manner, and impurities which are evenly distributed throughout particles. Use in conjunction with techniques such as thermal analysis and XRD would also detect impurities present as distinct phases or particles. Impurities are a common occurrence in multi-particle solid samples formed in process chemistry, but measurement of impurities usually provides just a total proportion of any specific impurity present. The approach described herein also allows the locations of impurities in samples to be evaluated, and so can be used to guide impurity management strategies. For example, recrystallisation or even improved washing may be successful in removing impurities shown to be localised on or near particle surfaces, whereas phase transformation or process chemistry redesign may be required for widely distributed impurities. To be industrially useful, the approach will need to be applied to samples containing much greater numbers of particles, requiring better anti-flocculation measures, based on either steric stabilisation using higher molecular weight or polymeric surfactants or electrostatic stabilisation,[38] and more sophisticated dissolution media.

Conclusions

The motivation for this work arises from the common occurrence of molecular impurities in pharmaceutical and fine chemical manufacturing and the use of crystallisation as the principle method of product isolation and purification.[4-8] In some instances, crystallisations are not sufficient to adequately remove impurities without an accompanying phase transformation or optimisation of the process chemistry,[9-18] in which cases the question of the location of impurities in crystalline batches arises. This is particularly the case when the impurity does not form a physically distinct phase which can be observed by XRD, thermal analysis or microscopy. In cases in which samples consist essentially of a single uniform phase subdivided into particles, impurities may exist at the level of individual molecules surrounded by

molecules of the crystallising compound. The concentration of such impurity molecules may be uniform or may vary, but in general has to be assumed to be a distribution which varies within particles and between particles. Formation of eutectics or other modes of incorporation are also possible.[47]

Previous work had shown that the distribution of such impurities could be mapped within large single crystals by a series of partial dissolutions with analysis of the solutions resulting from each dissolution step, and that such an approach could distinguish between relatively evenly and unevenly distributed impurities.[4,33,34] Such information could be very valuable in guiding impurity management during process development and troubleshooting. However, to be of value for process development and support, the approach needs to be applicable to samples of multiple particles. The present study aimed to examine the feasibility of such an approach. Quantities of 2-(2-ethylhexyloxy)ethanol, a low molecular weight compound with the essential features of a non-ionic surfactant, were added to inhibit agglomeration of the particles. Use of hexane as solvent, in which the crystallising compound, 2-nitro-4-trifluoromethylacetanilide (**1**), was poorly soluble at the temperatures of interest, provided a dissolution medium capable of dissolving only a proportion of each particle in any one step.

In order to test this approach, a system for study was required containing an impurity or impurities present at a reasonably predicable level and distribution. Use of a known solid solution system would be suitable in that an additive or impurity can be incorporated into the crystal lattice in a regular manner and at a known level. A system in which 2-nitro-4-trifluoromethylacetanilide (**1**) was the crystallising 'host' and 4-methyl-2-nitroacetanilide (**2**) and 4-chloro-2-nitroacetanilide (**3**)[32] were the 'guests' or 'impurities' was selected. In addition to additives **2** and **3**, which are known to act as isosteric lattice replacements in crystals of compound **1**, it was useful to have a comparison compound which was less likely to so act. Additive **4**, in which the acetamido group of compound **1** is replaced by the sterically demanding pivalamido group, was selected for this purpose.

As described above, the method showed that additives **2** and **3** were relatively evenly distributed throughout the crystals. In itself, that finding simply confirms that compounds **1**, **2** and **3** act as mutual isomorphic replacements, as has already been reported.[32] However, the approach which was employed could be applied to systems in which the result would not be predictable. The findings on the sterically demanding compound **4** show that less even distribution should also be determinable. There are clearly several aspects of the methods used

in this study which would need to be improved to provide an industry useful approach. The sample numbers are very small in comparison to realistic industrial test samples. In principle, the methodology can be expanded to larger samples by using more sophisticated dissolution media and more powerful anti-flocculation measures. However, once these deficiencies are addressed, the approach described herein can be used to map the distribution of impurities in batches of crystalline molecular chemicals, using conventional and widely available technologies such as liquid chromatography and particle sizing. Such data, in conjunction with standard thermal analysis, XRD and microscopy measurements would allow process chemists and engineers to make rational decisions on impurity management, process optimisation and trouble shooting.

Acknowledgements: This research has been carried out with the support of Science Foundation Ireland under Grant Number 12/RC/2275.

References

1. B. V. Petukhov, *Crystallography Reports*, 2007, **52**, 112-122.

2. M. D. McCluskey, *Journal of Applied Physics*, 2000, **87**, 3593-3617.

3. S. M. Myers, M. I. Baskes, H. K. Birnbaum, J. W. Corbett, G. G. DeLeo, S. K. Estreicher, E. E. Haller, P. Jena, N. M. Johnson, R. Kirchheim, S. J. Pearton, and M. J. Stavola, *Rev. Mod. Phys.,* 1992, **64**, 559-617.

4. H. A. Moynihan, D. E. Horgan, *Org. Proc. Res. Dev*., 2017, **21**, 689-704.

5. D. A. Pierson, B. A. Olsen, D. K. Robbins, K. M. DeVries, D. L. Varie, *Org. Proc. Res. Dev.,* 2009, **13**, 285-291.

6. J. P. Bercu, C. M. Callis, *Org. Proc. Res. Dev.,* 2009, **13**, 938-938.

7. S. N. Black, K. Quigley, A. Parker, *Org. Proc. Res. Dev.,* 2006, **10**, 241-244.

8. S. Black, L. Dang, C. Liu, H. Wei, *Org. Proc. Res. Dev.,* 2013, **17**, 486-492.

9. M. M. Hansen, D. J. Jarmer, E. Arslantas, A. C. DeBaillie, A. L. Frederick, M. Harding, D. W. Hoard, A. Hollister, D. Huber, S. P. Kolis, J. E. Kuenhe-Willmore, T. Kull, M. E. Laurila, R. J. Linder, T. J. Martin, J. R. Martinelli, M. J. McCulley, R. N. Richey, D. R. Starkey, J. A. Ward, N. Zaborenko, T. Zweifel, *Org. Proc. Res. Dev.,* 2015, **19**, 1214-1230.

10. X. Shi, H. Chang, M. Grohmann, W. F. Kiesman, D.-I. A. Kwok, *Org. Proc. Res. Dev.,* 2015**, 19**, 437-443.

11. B. P. Chekal, S. M. Guinness, B. M. Lillie, R. M. McLaughlin, C. W. Palmer, R. J. Post, J. E. Sieser, R. A. Singer, G. W. Sluggett, R. Vaidyanathan, G. W. Withbroe, *Org. Proc. Res. Dev.,* 2014, **18**, 266-274.

12. S. N. Black, M. W. Cuthbert, R. J. Roberts, *Cryst. Growth Des.,* 2004, **4**, 539-544.

13. N. Yoshikawa, F. Xu, J. D. Arrendondo, T. Itoh, *Org. Proc. Res. Dev.,* 2011, **15**, 824-830.

14. A. Isidro-Llobet, M. Alverez, F. Albericio, *Chem. Rev.,* 2009, **109**, 2455-2504.

15. S. Sankareswaran, M. Mannam, V. Chakka, S. R. Mandapati, P. Kumar, *Org. Proc. Res. Dev.,* **2016**, 20, 1461-1468.

16. A. Stumpf, A. McClory, H. Yajima, N. Segraves, R. Angelaud, F. Gosselin, *Org. Proc. Res. Dev.,* 2016**, 20**, 751-759.

17. S. Duan, D. Place, H. H. Perfect, N. D. Ide, M. Maloney, K. Sutherland, K. E. Price Wiglesworth, K. Wang, M. Olivier, F. Kong, K. Leeman, J. Blunt, J. Draper, M. McAuliffe, M. O'Sullivan, D. Lynch, *Org. Proc. Res. Dev.,* 2016, **20**, 1191-1202.

18. Q. Wen, J. Jin, L. Zhang, Y. Luo, P. Lu, Y. Wang, *Tetrahedron Letters*, 2014, **55**, 1271-1280.

19. C. G. Moyers, *Chem. Eng. Prog.,* 1986, **82**, 42-46.

20. J. A. Hayes, K. S. Eccles, S. E. Lawrence, H. A. Moynihan, *Carbohydr. Res.*, 2012, **349**, 108-112.

21. G. J. Tanoury, R. Hett, D. W. Kessler, S. A. Wald, C. H. Sennayake, *Org. Proc. Res. Dev.,* 2002, **6**, 855-862.

22. N. Blagden, *Powder Technology,* 2001, **121**, 46-52.

23. K. A. Solanko, A. D. Bond, *CrystEngComm,* 2011, **13**, 6991-6996.

24. T. Mukuta, A. Y. Lee, T. Kawakami, A. S. Myerson, *Cryst. Growth Des.*, 2005, **5**, 1429-1436.

25. M. Mirmehrabi, S. Rohani, K. S. K. Murthy, B. Radatus, *Cryst. Growth Des.,* 2006, **6**, 141-149.

26. Z. Berkovitch-Yellin, L. Addadi, M. Idelson, M. Lahav, L. Leiserowitz, *Angew. Chem. Suppl.,* 1982, 1336-1345.

27. N. Blagden, M. Song, R. J. Davey, L. Seton, C. C. Seaton, *Cryst. Growth Des.*, 2005, **5**, 467-471.

28. Y. Deng, Q. Xie, M. G. LaPoprte, A. T. A. Chasnoff, M. A. Mortensen, D. Patra, S. A. Putrelo, R. S. Antonovich, H. Coa, Y. Yan, A. J. Cooper, S. R.; Rippin, M. D. Alexander, P. T. Kumar, M. S. Hendi, Y-. H. Lee, T. Hainmowitz, S. M. Condon, *Org. Proc. Res. Dev.,* 2016, **20**, 242-252.

29. M. T. Maloney, B. P. Jones, M. A. Olivier, J. Magano, K. Wang, N. D. Ide, A. S. Palm, D. R. Bill, K. R. Leeman, K. Sutherland, J. Draper, A. M. Daly, J. Keane, D. Lynch, M. O'Brien, J. Touhy, *Org. Proc. Res. Dev.*, 2016, **20**, 1203-1216.

30. B. Y. Shekunov, S. Bristow, A. H. L. Chow, L. Cranswick, D. J. W. Grant, P. York, *Cryst. Growth Des.,* 2003, **3**, 603-610.

31. H. Kaemmerer, H. Lorenz, S. N. Black, A. Seidel-Morgenstern, *Cryst. Growth Des.,* 2009, **9**, 1851-1862.

32. X. He, J. G. Stowell, K. R. Morris, R. R. Pfeiffer, H. Lui, P. Stahly, S. R. Byrn, *Cryst. Growth Des.,* 2001, **1**, 305-312.

33. L. Addadi, S. Weinstein, E. Gati, I. Weissbuch, M. Lahav, *J. Am. Chem. Soc.,* 1982, **104**, 4610-4617.

34. D. E. Horgan, L. M. Crowley, S. P. Stokes, S. E. Lawrence, H. A. Moynihan, from "Crystallization" by Y. Mastai (Ed.), InTech, 2015, Rijeka, Croatia; ISBN 978-953-51-2125-1.

35. G. Berti., G. Catelani,, B. Lombardi, L. Monti, *Gazz. Chim. Ital.,* 1977, **107**, 175-180.

36. A. V. Zeiger, M. M. Joullié, *J. Org. Chem.,* 1977, **42**, 542-545.

37. A. J. Gordon, R. A. Ford, from "The Chemist's Companion: A Handbook of Practical Data, Techniques, and References"; A. J. Gordon, R. A. Ford, Eds.; Wiley: New York, 1972; p 109.

38. D. H. Napper, *Ind. Eng. Chem. Prod. Res. Develop*., 1970, **9**, 467-477.

39. M. Oijima, N. Okamura, J. Tatami, *Ind. Eng. Chem. Res.,* 2015, **54**, 12847-12854.

40. C. Knieke, A. S. Azad, R. N. Davé, E. Bilgile, *Chem. Eng. Res. Design*, 2013, **91**, 1245-1258.

41. A. Dokoumetzidis, P. Macheras, *Int. J. Pharm.,* 2006, **321**, 1-11.

42. A. P. Tinke, K. Vanhoutte, R. De Maesschalck, S. Verheyen, H. De Winter, *J. Pharm. Biomed. Anal.,* 2005, **39**, 900-907.

43. H. Katepalli, A. Bose, T. A. Hatton, D. Blankschtein, *Langmuir*, 2016, **32**, 10694-10698.

44. T. Schnidts, P. Schluoo, A. Gross, D. Dobler, F. Runkel, *J. Dispersion Sci. Technol.,* 2012, **33**, 816-820.

45. D. Smrcka, J. Dohnal, F. Stepanek, *Eur. J. Pharmaceutics and Biopharm.,* 2016, **106**, 107-116.

46. M. Kitamura, T. Nakai, *J. Chem. Eng. Jpn.,* 1983, **16**, 288-293.

47. S. Cherukuvada, A. Nangia, *Chem. Commum.,* 2014, **50**, 906-923.

Determination of composition distributions of multi-particle crystalline samples by sequential dissolution with concomitant particle sizing and solution analysis

Humphrey A. Moynihan* and Declan Armstrong

School of Chemistry / Analytical and Biological Chemistry Research Facility / Synthesis and Solid-state Pharmaceutical Centre, University College Cork, College Road, Cork, TY12 YN60, Republic of Ireland.

h.moynihan@ucc.ie

SUPPLEMENTARY INFORMATION

Contents

Synthesis of *N*-(2-nitro-4-trifluoromethylphenyl)pivalamide (4): page 4

Figure S1. 1H NMR spectrum of *N*-(2-nitro-4-trifluoromethylphenyl)pivalamide (**4**)**:** page 5

Figure S2. ^{13}C NMR {^{1}H} spectrum of *N*-(2-nitro-4-trifluoromethylphenyl)pivalamide (**4**)**:** page 5

Figure S3. ^{19}F NMR {^{1}H} spectrum of *N*-(2-nitro-4-trifluoromethylphenyl)pivalamide (**4**)**:** page 6

HPLC Calibration Data: pages 7 - 9

Figure S4. TGA curve overlaid the DSC curve for **1** doped with 8 mol % of **4**: page 10

Figure S5. Chart comparing particle area versus the ranking of each particle in a partial dissolution series of **1** doped with 0.5 mol % of **2**: page 10

Figure S6. Chart comparing particle length versus the ranking of each particle in a partial dissolution series of **1** doped with 0.5 mol % of **2**: page 11

Figure S7. Chart comparing particle area versus the ranking of each particle in a partial dissolution series of **1** doped with 1.0 mol % of **2**: page 11

Figure S8. Chart comparing particle length versus the ranking of each particle in a partial dissolution series of **1** doped with 1.0 mol % of **2**: page 12

Figure S9. Chart comparing particle length versus the ranking of each particle in a partial dissolution series of **1** doped with 1.5 mol % of **2**: page 12

Figure S10. Chart comparing particle area versus the ranking of each particle in a partial dissolution series of **1** doped with 2.0 mol % of **2**: page 13

Figure S11. Chart comparing particle length versus the ranking of each particle in a partial dissolution series of **1** doped with 2.0 mol % of **2**: page 13

Figure S12. Chart comparing particle area versus the ranking of each particle in a partial dissolution series of **1** doped with 2.5 mol % of **2**: page 14

Figure S13. Chart comparing particle length versus the ranking of each particle in a partial dissolution series of **1** doped with 2.5 mol % of **2**: page 13

Figure S14. Chart comparing particle area versus the ranking of each particle in a partial dissolution series of **1** doped with 3.0 mol % of **2**: page 15

Figure S15. Chart comparing particle length versus the ranking of each particle in a partial dissolution series of **1** doped with 3.0 mol % of **2**: page 15

Figure S16. Chart comparing particle area versus the ranking of each particle in a partial dissolution series of **1** doped with 0.5 mol % of **3:** page 16

Figure S17. Chart comparing particle length versus the ranking of each particle in a partial dissolution series of **1** doped with 0.5 mol % of **3**: page 16

Figure S18. Chart comparing particle area versus the ranking of each particle in a partial dissolution series of **1** doped with 1.0 mol % of **3**: page 17

Figure S19. Chart comparing particle length versus the ranking of each particle in a partial dissolution series of **1** doped with 1.0 mol % of **3**: page 17

Figure S20. Chart comparing particle area versus the ranking of each particle in a partial dissolution series of **1** doped with 1.5 mol % of **3**: page 18

Figure S21. Chart comparing particle length versus the ranking of each particle in a partial dissolution series of **1** doped with 1.5 mol % of **3**: page 18

Figure S22. Chart comparing particle area versus the ranking of each particle in a partial dissolution series of **1** doped with 2.0 mol % of **3**: page 19

Figure S23. Chart comparing particle length versus the ranking of each particle in a partial dissolution series of **1** doped with 2.0 mol % of **3**: page 19

Figure S24. Chart comparing particle length versus the ranking of each particle in a partial dissolution series of **1** doped with 2.5 mol % of **3**: page 20

Figure S25. Chart comparing particle area versus the ranking of each particle in a partial dissolution series of **1** doped with 3.0 mol % of **3**. Page 20

Figure S26. Chart comparing particle length versus the ranking of each particle in a partial dissolution series of **1** doped with 3.0 mol % of **3**: page 21

Figure S27. Plot of percentage by HPLC of added impurity in crystals of compound **1** *vs.* the dissolution mid-point for the sample of crystals grown from solutions containing 0.5 mol % of additive **2**: page 21

Figure S28. Plot of percentage by HPLC of added impurity in crystals of compound **1** *vs.* the dissolution mid-point for the sample of crystals grown from solutions containing 1.0 mol % of additive **2**: page 22

Figure S29. Plot of percentage by HPLC of added impurity in crystals of compound **1** *vs.* the dissolution mid-point for the sample of crystals grown from solutions containing 2.0 mol % of additive **2**: page 22

Figure S30. Plot of percentage by HPLC of added impurity in crystals of compound **1** *vs.* the dissolution mid-point for the sample of crystals grown from solutions containing 2.5 mol % of additive **2** page 23

Figure S31. Plot of percentage by HPLC of added impurity in crystals of compound **1** *vs.* the dissolution mid-point for the sample of crystals grown from solutions containing 3.0 mol % of additive **2**: page 23

Figure S32. Plot of percentage by HPLC of added impurity in crystals of compound **1** *vs.* the dissolution mid-point for the sample of crystals grown from solutions containing 0.5 mol % of additive **3**: page 24

Figure S33. Plot of percentage by HPLC of added impurity in crystals of compound **1** *vs.* the dissolution mid-point for the sample of crystals grown from solutions containing 1.0 mol % of additive **3**: page 24

Figure S34. Plot of percentage by HPLC of added impurity in crystals of compound **1** *vs.* the dissolution mid-point for the sample of crystals grown from solutions containing 1.5 mol % of additive **3**: page 25

Figure S35. Plot of percentage by HPLC of added impurity in crystals of compound **1** *vs.* the dissolution mid-point for the sample of crystals grown from solutions containing 2.0 mol % of additive **3**: page 25

Figure S36. Plot of percentage by HPLC of added impurity in crystals of compound **1** *vs.* the dissolution mid-point for the sample of crystals grown from solutions containing 3.0 mol % of additive **3**: page 26

Figure S37. Plot of percentage by HPLC of added impurity in a single crystal of compound **1**, grown from solutions containing 3.0 mol % of additive **3**, *vs.* the dissolution mid-point for the crystal: page 27

Synthesis of *N*-(2-nitro-4-trifluoromethylphenyl)pivalamide 4

N-(2-nitro-4-trifluoromethylphenyl)pivalamide **4** was prepared by heating a mixture of 2-nitro-4-trifluoromethylaniline (1.0 g, 4.852 mmol), trimethylacetic anhydride (1.5 mL, 7.390 mmol), and two drops of sulphuric acid to 80 °C for 3 hours. The resulting solution was allowed to cool to room temperature with the formation of yellow plate-like crystals. Water (10 mL) was added to the reaction mixture, and with manual stirring further solid precipitated out of solution. The crude product was isolated by vacuum filtration, washed with two 10 mL portions of water and air dried. The crude product was purified by recrystallization with 20 mL of ethanol, isolated by vacuum filtration, washed with a further 10 mL of ice-cold ethanol and air dried. Yield 0.462 g (33 %) of a yellow crystalline solid. M.p. 92 - 94 °C. ^{1}H NMR (300 MHz, $CDCl_3$): δ 10.89 (1H, s, N*H*), 9.05 (1H, d, $^{3}J_{HH}$ = 9 Hz, H6), 8.52 (1H, d, $^{4}J_{HH}$ = 2 Hz, H3), 7.87 (1H, dd, $^{3}J_{HH}$ = 9, $^{4}J_{HH}$ = 2 Hz, H5), 1.37 (s, 9H, 3 × C*H*$_3$) ppm; ^{13}C{^{1}H} NMR (DEPTQ-135) (75 MHz, $CDCl_3$): δ 178.17 (s, *C*=O), 138.37 (s, C1), 135.54 (s, C2), 132.43 (q, $^{3}J_{CF}$ = 3.3 Hz, C5), 124.86 (q, $^{2}J_{CF}$ = 34.6 Hz, C4), 123.77 (q, $^{1}J_{CF}$ = 272.1 Hz, *C*F$_3$), 123.51 (q, $^{3}J_{CF}$ = 4.1 Hz, C3), 122.67 (s, C6), 40.91 (s, *C*(CH$_3$)$_3$), 27.43 (s, 3 × *C*H$_3$) ppm; ^{19}F{^{1}H} NMR (282 MHz, $CDCl_3$): δ -62.65 (s, C*F*$_3$) ppm. ESI-MS (CH_3CN): 291.2 positive mode [M + H$^+$, calc. 291.10 for $C_{12}H_{14}N_2F_3O_3$]; 292.2 positive mode [M + H$^+$ + 1, calc. 292.10 for $C_{12}H_{14}N_2F_3O_3$]; 289.2 negative mode [M - H, calc. 289.08 for $C_{12}H_{12}N_2F_3O_3$]; 290.3 negative mode [M - H + 1, calc. 290.09 for $C_{12}H_{12}N_2F_3O_3$] R_f (1:7 ethyl acetate:hexane on silica gel) = 0.55.

[^{1}H (300 MHz), ^{13}C{^{1}H} (75 MHz), and ^{19}F{^{1}H} NMR (282 MHz) spectra were recorded on a Bruker Avance 300 MHz NMR spectrometer. Low resolution mass spectra were recorded on a Waters Quattro Micro triple quadrupole instrument in electrospray ionization (ESI) mode using 50% acetonitrile-water containing 0.1% formic acid as eluent; samples were prepared in acetonitrile.]

NMR

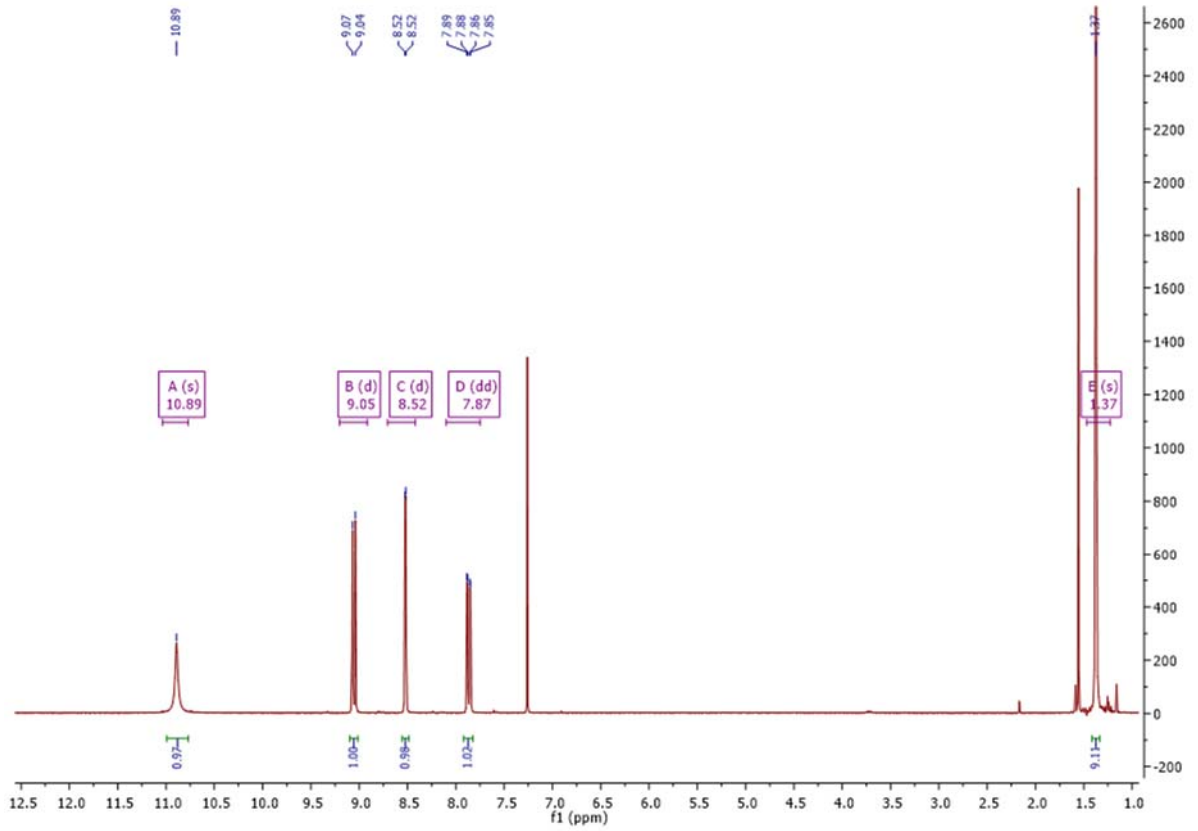


Figure S1. ^{1}H NMR spectrum of **4** in $CDCl_3$.

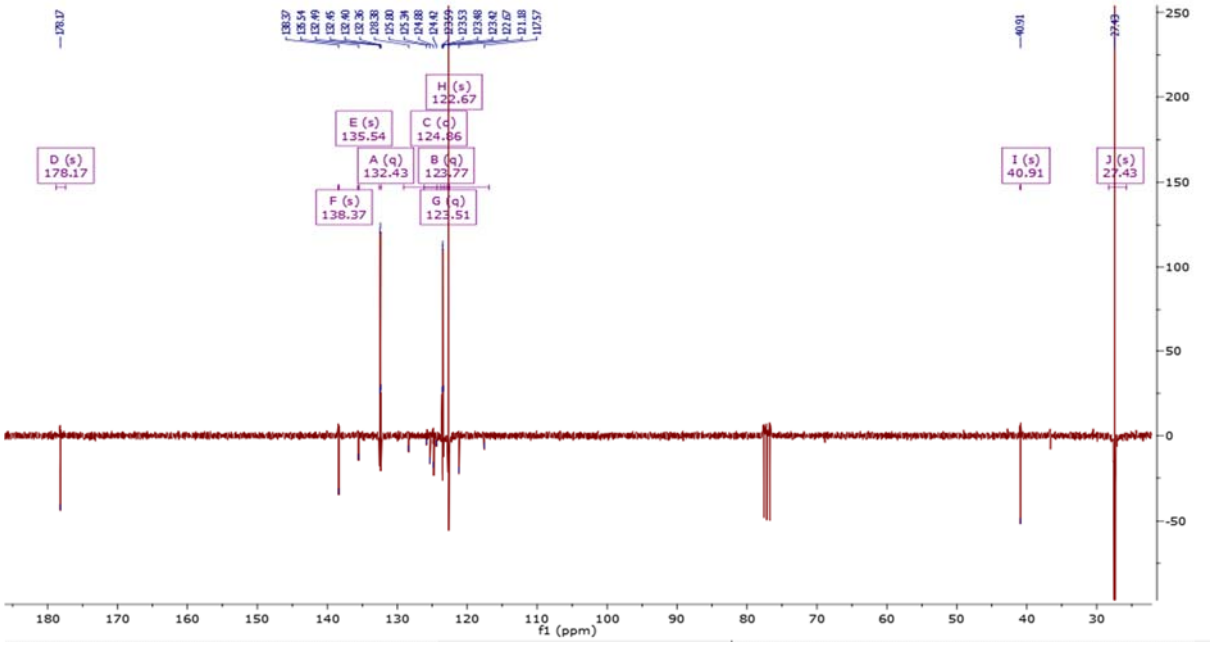


Figure S2. ^{13}C NMR {^{1}H} (DEPTQ-135) spectrum of **4** in $CDCl_3$. CH and CH_3 signals are positive, all other signals are negative.

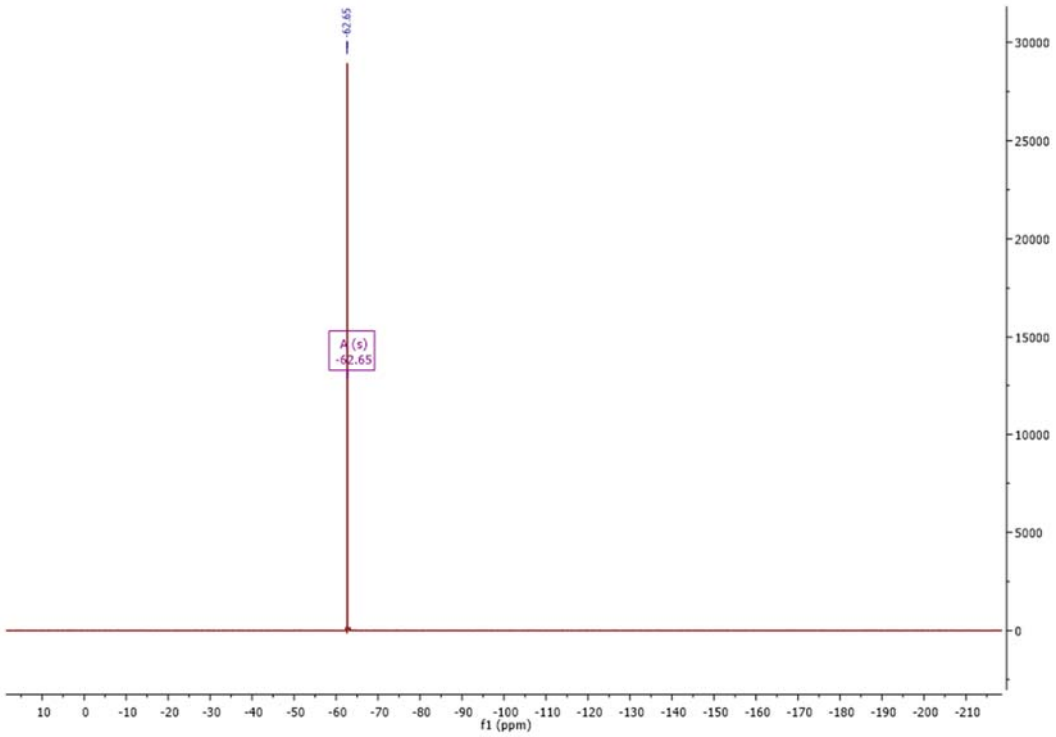


Figure S3. ^{19}F NMR $\{^{1}H\}$ spectrum of **4** in $CDCl_3$.

HPLC Calibration Data

General Calibration Setting

```
Calib. Data Modified  :      21-Jun-17 12:24:13 PM
Signals calculated separately :      No
Rel. Reference Window :      5.000 %
Abs. Reference Window :      0.000 min
Rel. Non-ref. Window  :      5.000 %

Abs. Non-ref. Window  :      0.000 min
Uncalibrated Peaks    :      not reported
Partial Calibration   :      Yes, identified peaks are recalibrated
Correct All Ret. Times:      No, only for identified peaks
Curve Type            :      Linear
Origin                :      Forced
Weight                :      Equal
Recalibration Settings:
Average Response      :      Average all calibrations
Average Retention Time:      Floating Average New 75%
```

Signal Details

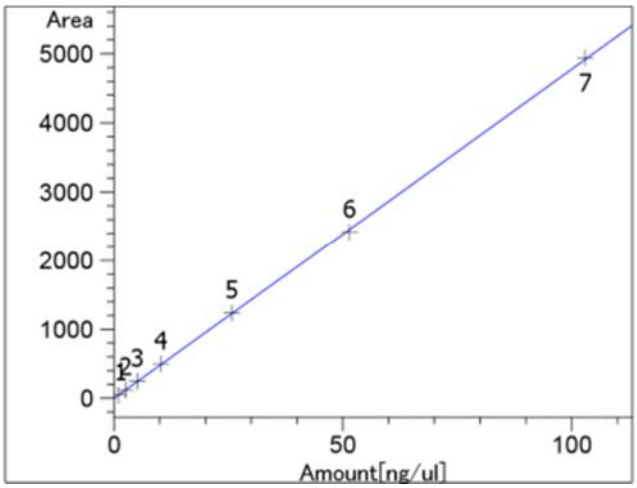
Signal 1: DAD1 A, Sig=234,4 Ref=360,100

Overview Table

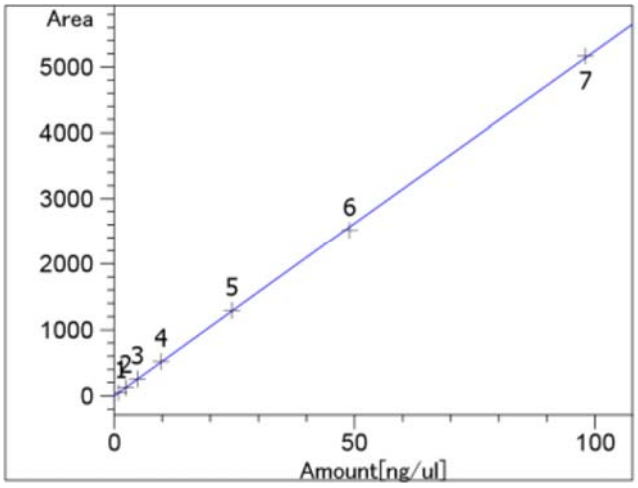
RT	Sig	Lvl	Amount [ng/ul]	Area	Rsp.Factor	Ref	ISTD	#	Compound
5.059	1	1	1.03000	47.69269	2.15966e-2	No	No	**2**	
		2	2.57500	120.68970	2.13357e-2				
		3	5.15000	246.91501	2.08574e-2				
		4	10.30000	497.15610	2.07178e-2				
		5	25.75000	1238.43115	2.07924e-2				
		6	51.50000	2416.96289	2.13077e-2				
		7	103.00000	4937.32324	2.08615e-2				
6.990	1	1	9.80000e-1	50.16642	1.95350e-2	No	No	**3**	
		2	2.45000	125.26588	1.95584e-2				
		3	4.90000	257.21909	1.90499e-2				
		4	9.80000	518.87018	1.88872e-2				
		5	24.50000	1292.15259	1.89606e-2				
		6	49.00000	2516.06958	1.94748e-2				
		7	98.00000	5164.98242	1.89739e-2				
12.732	1	1	1.02000	48.12077	2.11967e-2	No	No	**1**	
		2	2.55000	113.33391	2.24999e-2				
		3	5.10000	230.78233	2.20987e-2				
		4	10.20000	465.83960	2.18959e-2				
		5	25.50000	1158.93127	2.20030e-2				
		6	51.00000	2261.68774	2.25495e-2				
		7	102.00000	4634.19922	2.20103e-2				
23.282	1	1	1.02000	34.24325	2.97869e-2	No	No	**4**	
		2	2.55000	86.07143	2.96266e-2				
		3	5.10000	175.30609	2.90920e-2				
		4	10.20000	354.45395	2.87767e-2				
		5	25.50000	883.34070	2.88677e-2				

6	51.00000	1717.42346	2.96956e-2
7	102.00000	3517.49609	2.89979e-2

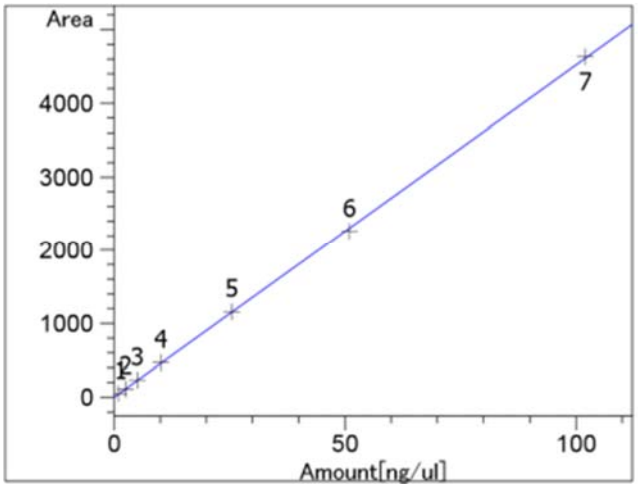
Calibration Curves



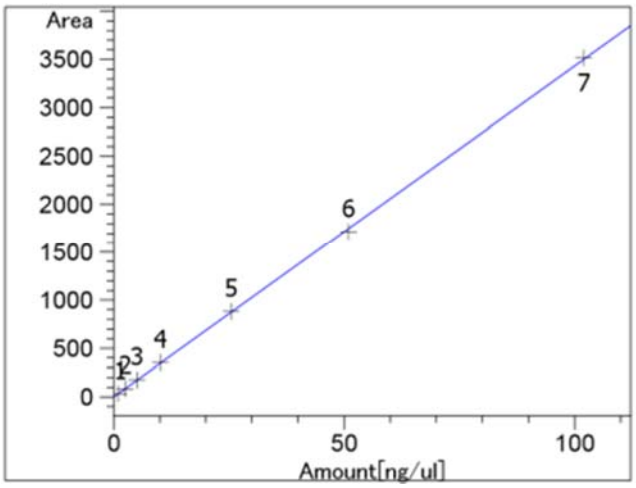
2 at exp. RT: 5.070
DAD1 A, Sig=234,4 Ref=360,100
Correlation: 0.99996
Residual Std. Dev.: 19.39276
Formula: y = mx
m: 47.75528
x: Amount[ng/ul]
y: Area



3 at exp. RT: 7.003
DAD1 A, Sig=234,4 Ref=360,100
Correlation: 0.99995
Residual Std. Dev.: 24.56110
Formula: y = mx
m: 52.45060
x: Amount[ng/ul]
y: Area



1 at exp. RT: 12.745
DAD1 A, Sig=234,4 Ref=360,100
Correlation: 0.99996
Residual Std. Dev.: 20.48602
Formula: y = mx
m: 45.23025
x: Amount[ng/ul]
y: Area



4 at exp. RT: 23.275
DAD1 A, Sig=234,4 Ref=360,100
Correlation: 0.99996
Residual Std. Dev.: 15.54065
Formula: y = mx
m: 34.34116
x: Amount[ng/ul]
y: Area

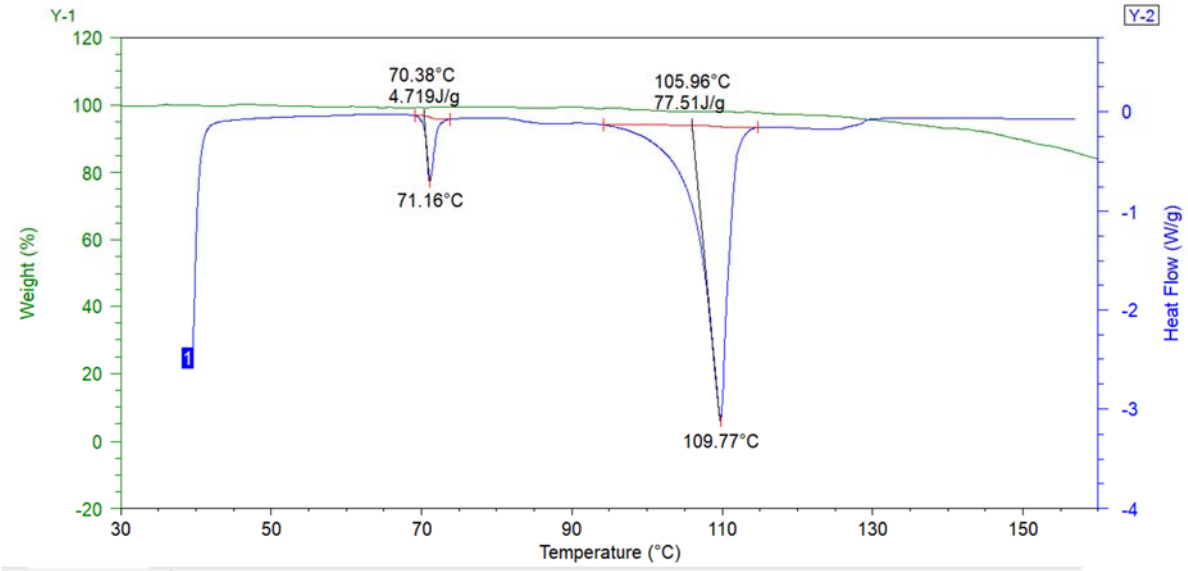


Figure S4. TGA curve overlaid the DSC curve for **1** doped with 8 mol % of **4**.

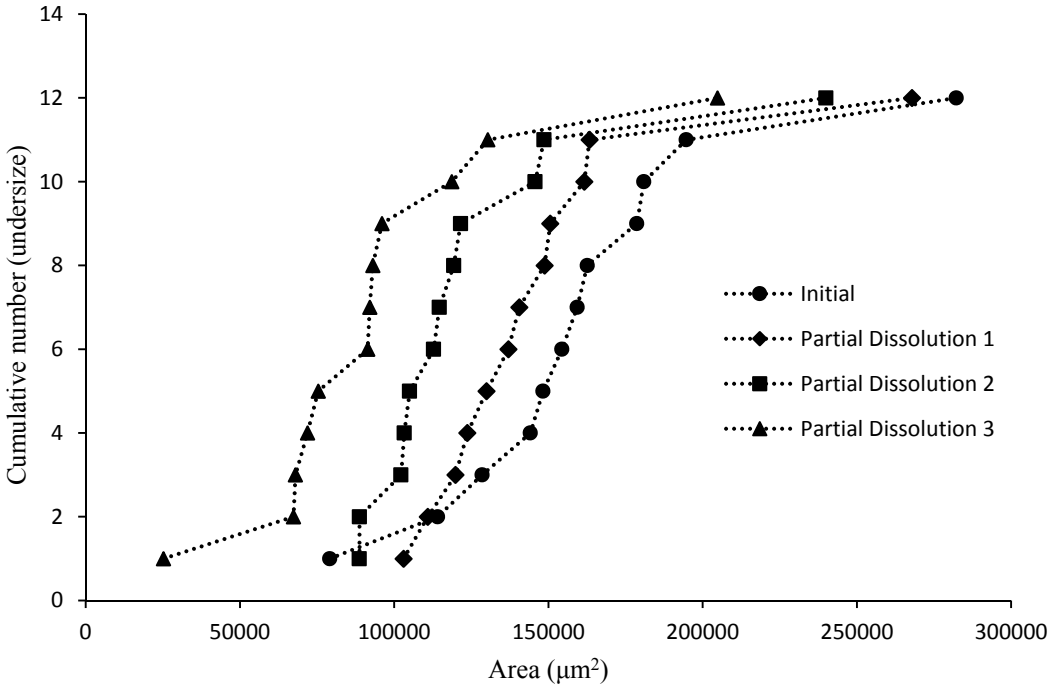


Figure S5. Chart comparing particle area versus the ranking of each particle in a partial dissolution series of **1** doped with 0.5 mol % of **2**.

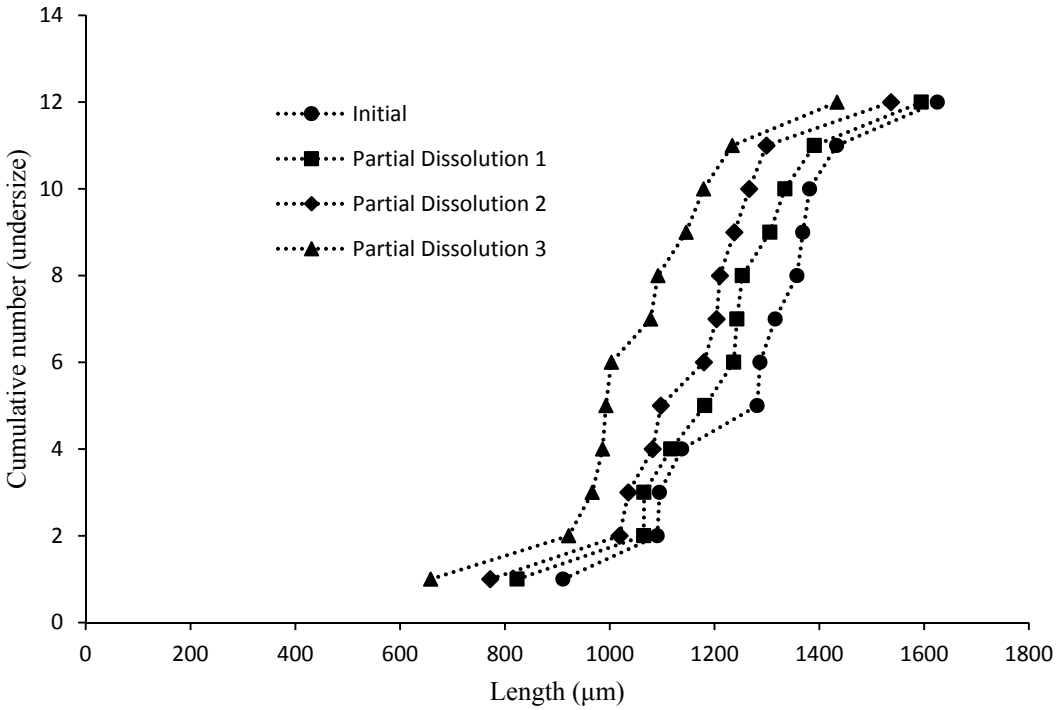


Figure S6. Chart comparing particle length versus the ranking of each particle in a partial dissolution series of **1** doped with 0.5 mol % of **2**.

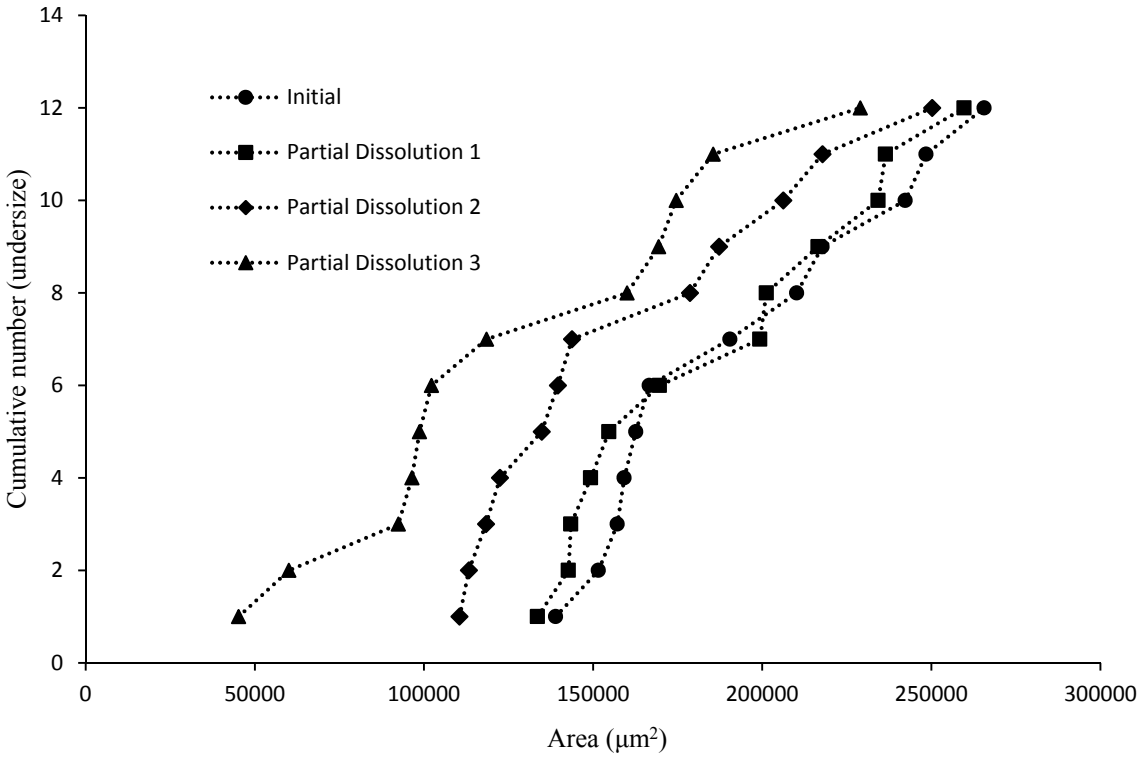


Figure S7. Chart comparing particle area versus the ranking of each particle in a partial dissolution series of **1** doped with 1.0 mol % of **2**.

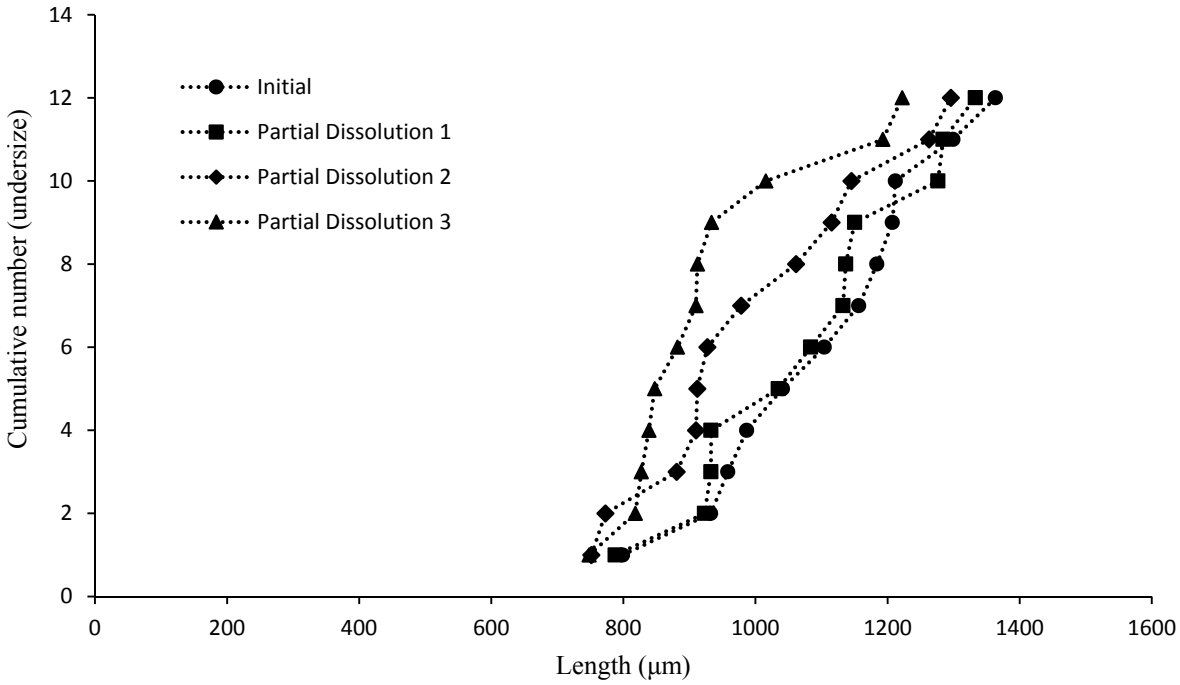


Figure S8. Chart comparing particle length versus the ranking of each particle in a partial dissolution series of **1** doped with 1.0 mol % of **2**.

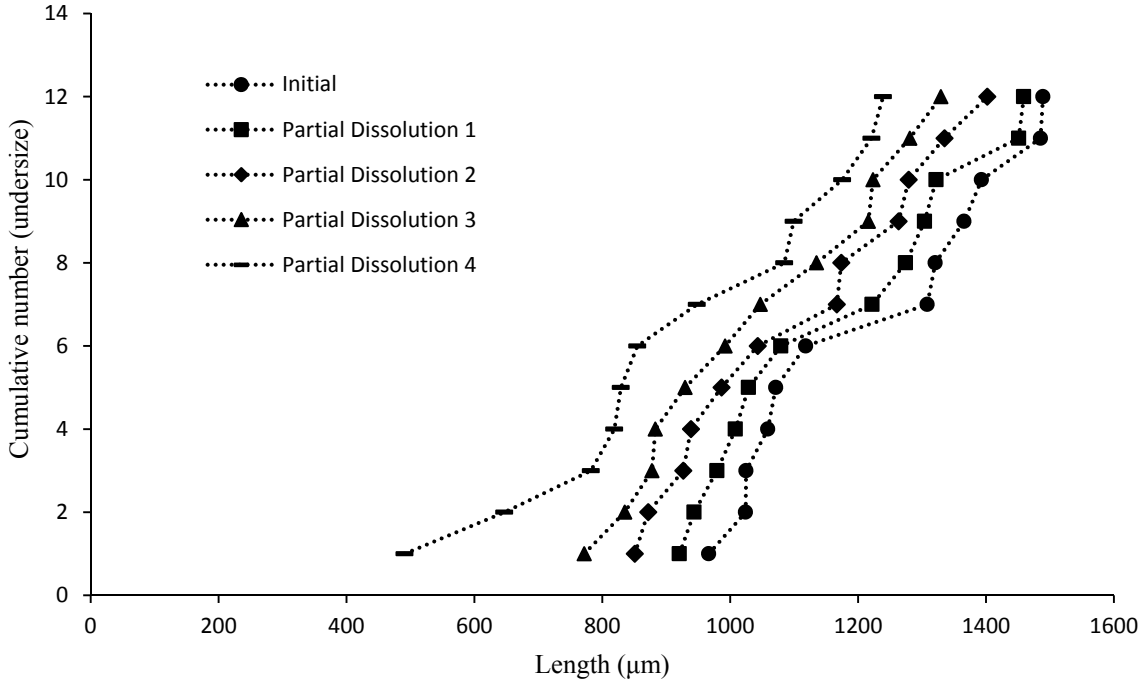


Figure S9. Chart comparing particle length versus the ranking of each particle in a partial dissolution series of **1** doped with 1.5 mol % of **2**.

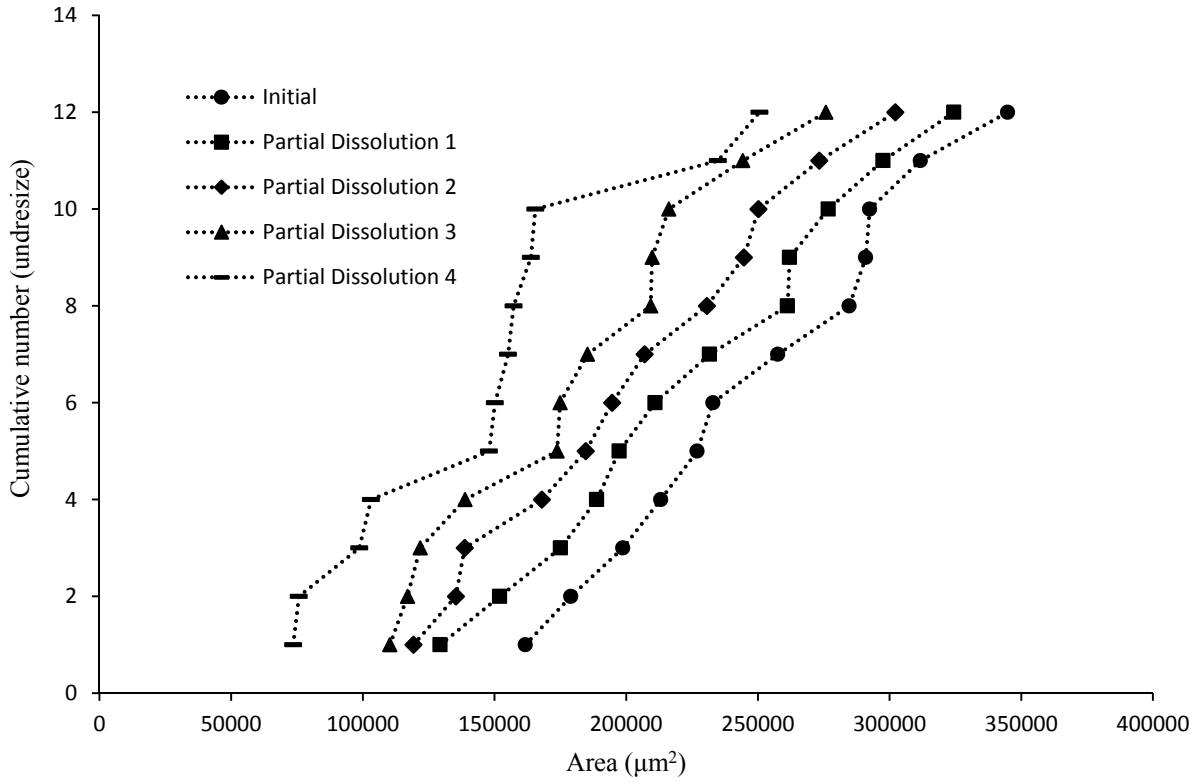


Figure S10. Chart comparing particle area versus the ranking of each particle in a partial dissolution series of **1** doped with 2.0 mol % of **2**.

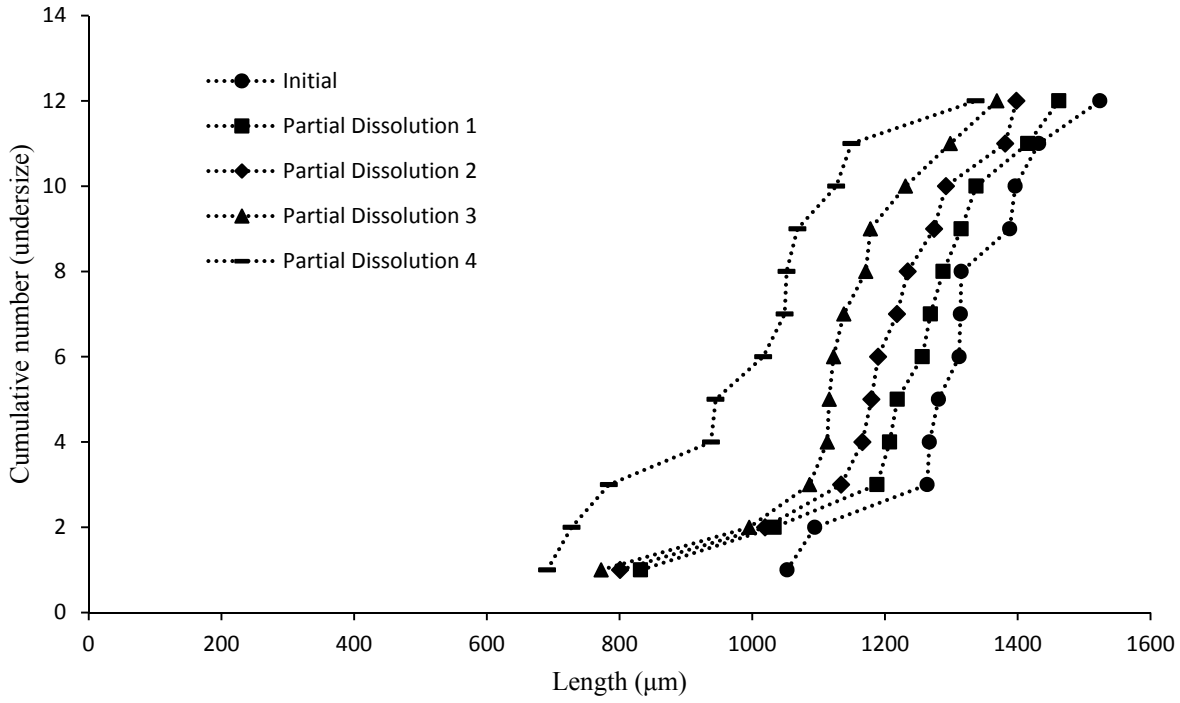


Figure S11. Chart comparing particle length versus the ranking of each particle in a partial dissolution series of **1** doped with 2.0 mol % of **2**.

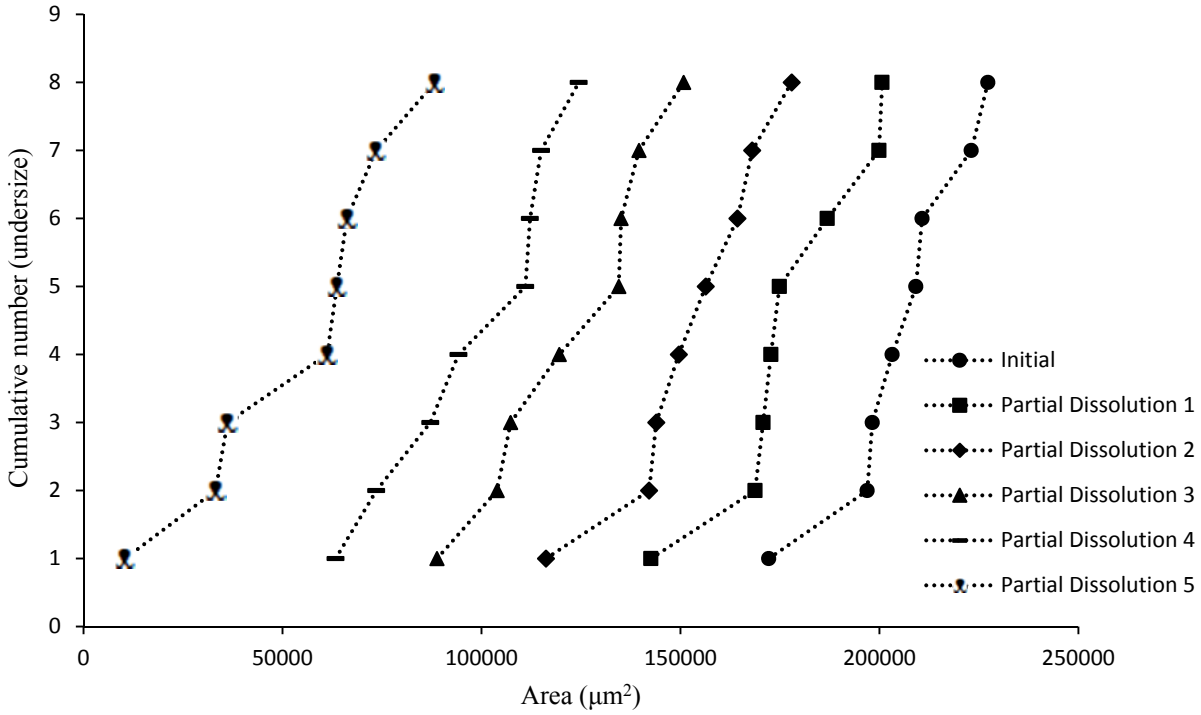


Figure S12. Chart comparing particle area versus the ranking of each particle in a partial dissolution series of **1** doped with 2.5 mol % of **2**.

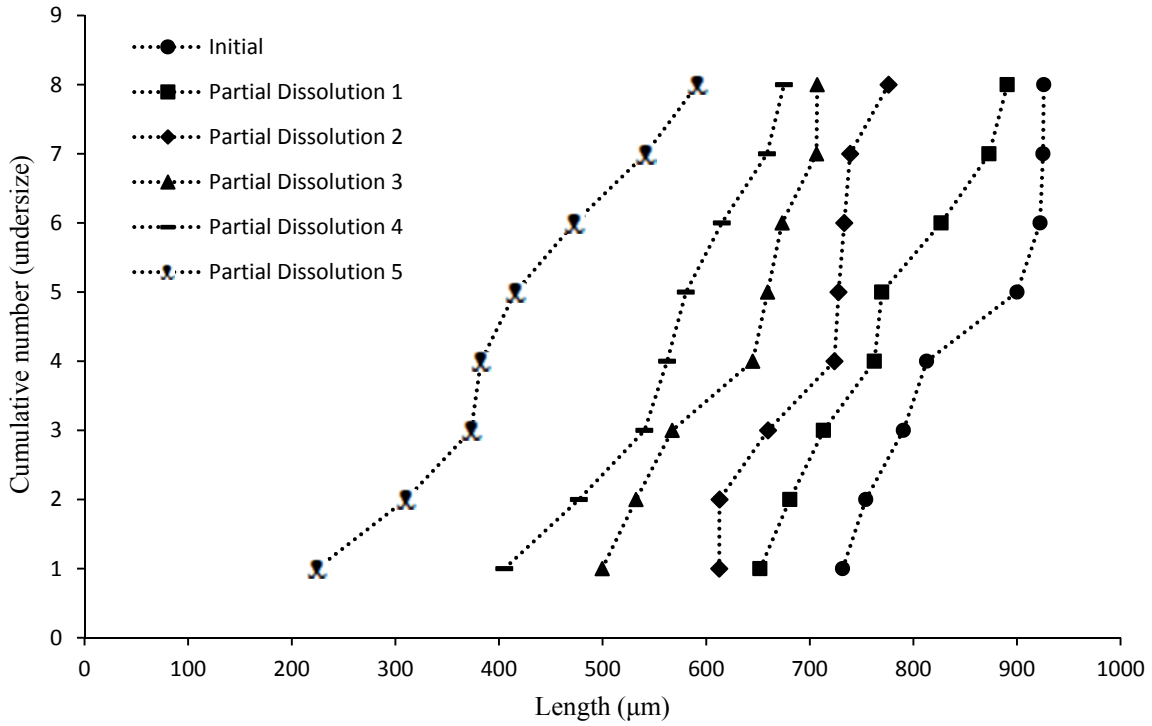


Figure S13. Chart comparing particle length versus the ranking of each particle in a partial dissolution series of **1** doped with 2.5 mol % of **2**.

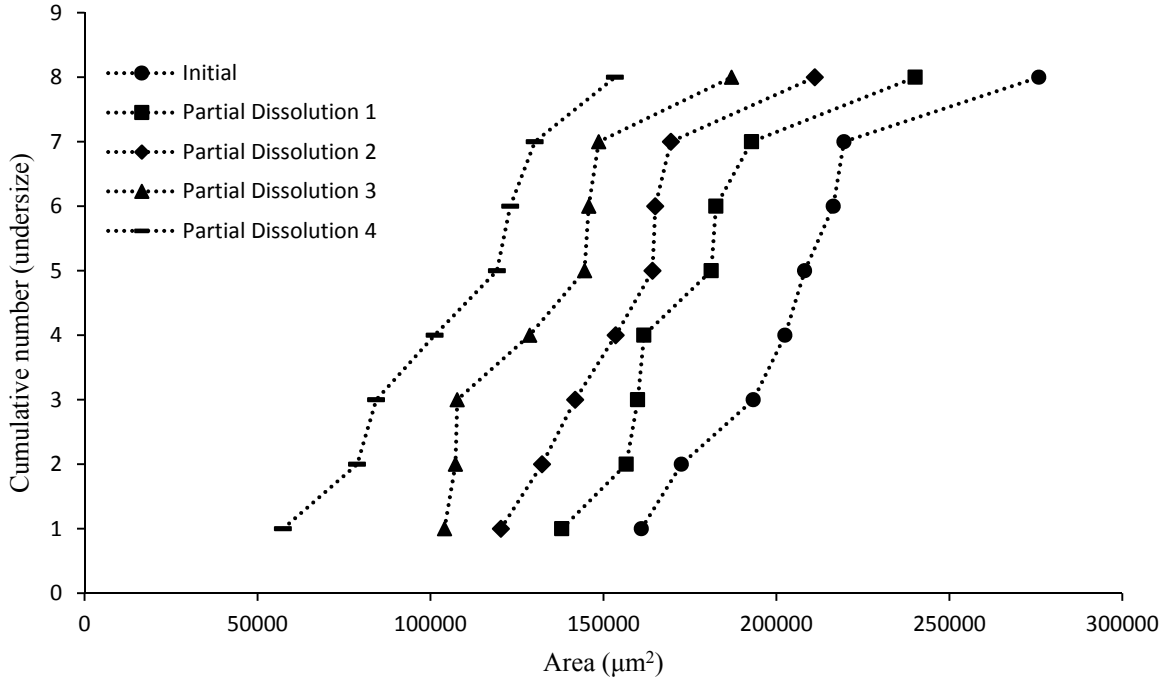


Figure S14. Chart comparing particle area versus the ranking of each particle in a partial dissolution series of **1** doped with 3.0 mol % of **2**.

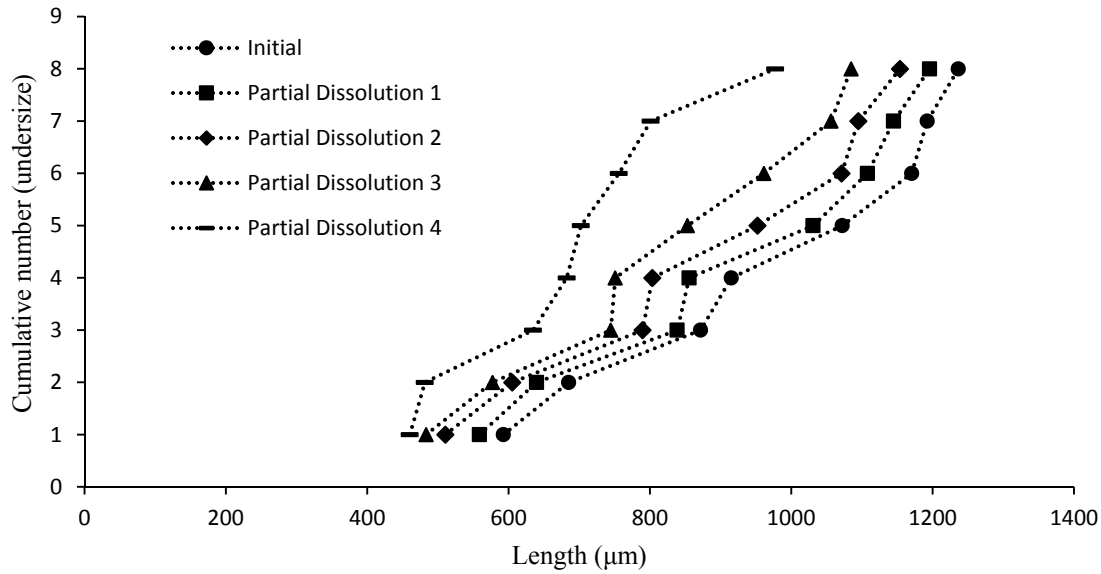


Figure S15. Chart comparing particle length versus the ranking of each particle in a partial dissolution series of **1** doped with 3.0 mol % of **2**.

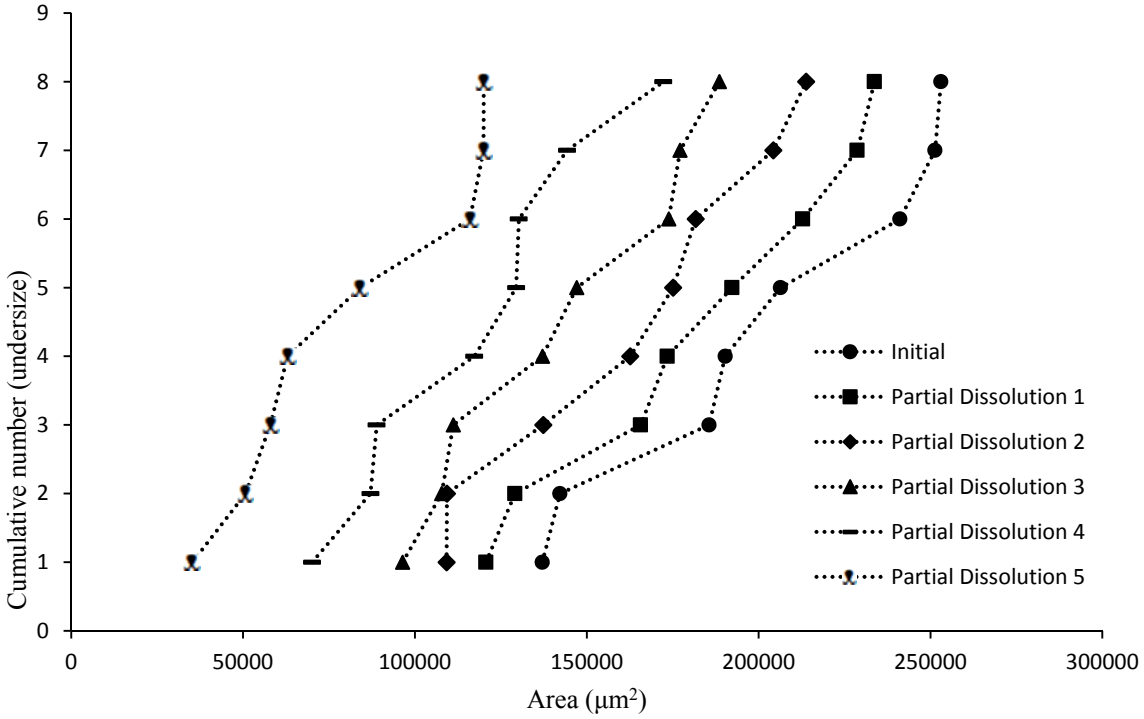


Figure S16. Chart comparing particle area versus the ranking of each particle in a partial dissolution series of **1** doped with 0.5 mol % of **3**.

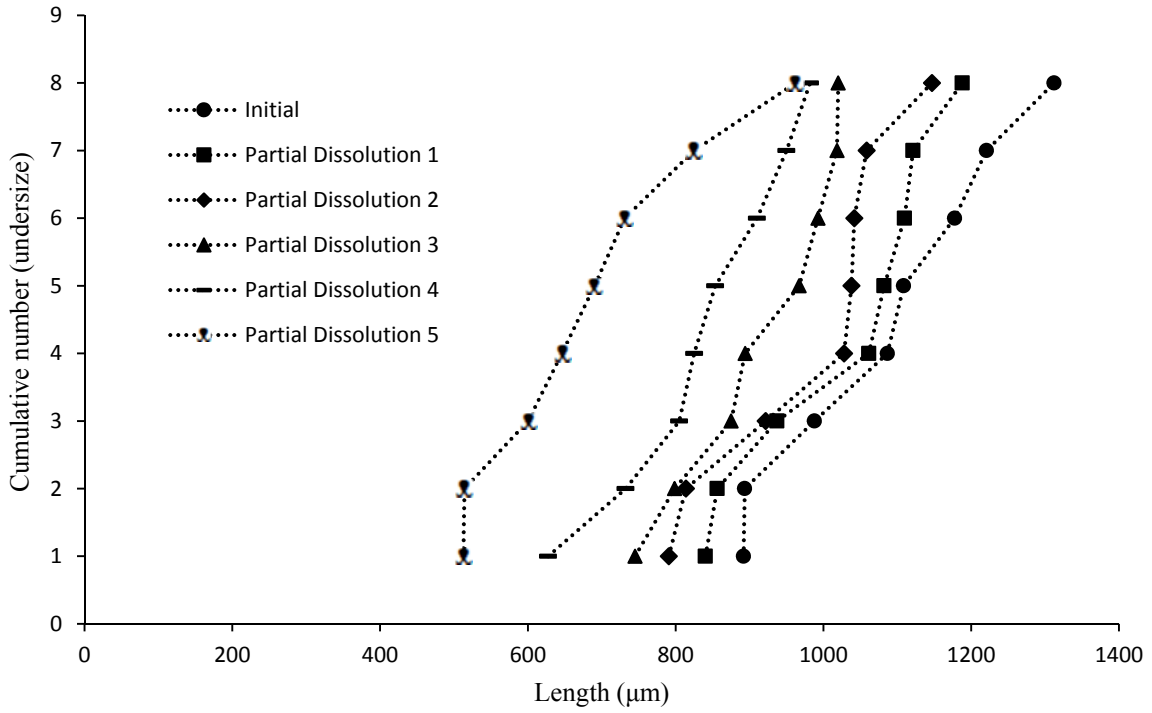


Figure S17. Chart comparing particle length versus the ranking of each particle in a partial dissolution series of **1** doped with 0.5 mol % of **3**.

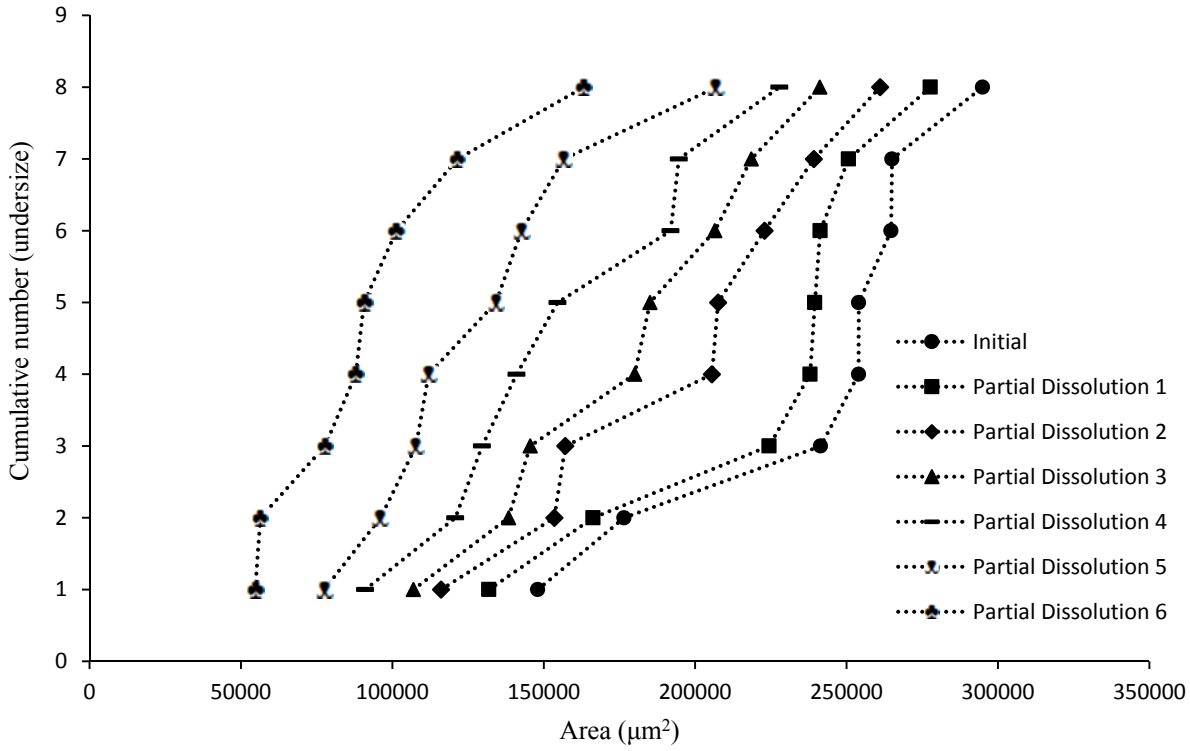


Figure S18. Chart comparing particle area versus the ranking of each particle in a partial dissolution series of **1** doped with 1.0 mol % of **3**.

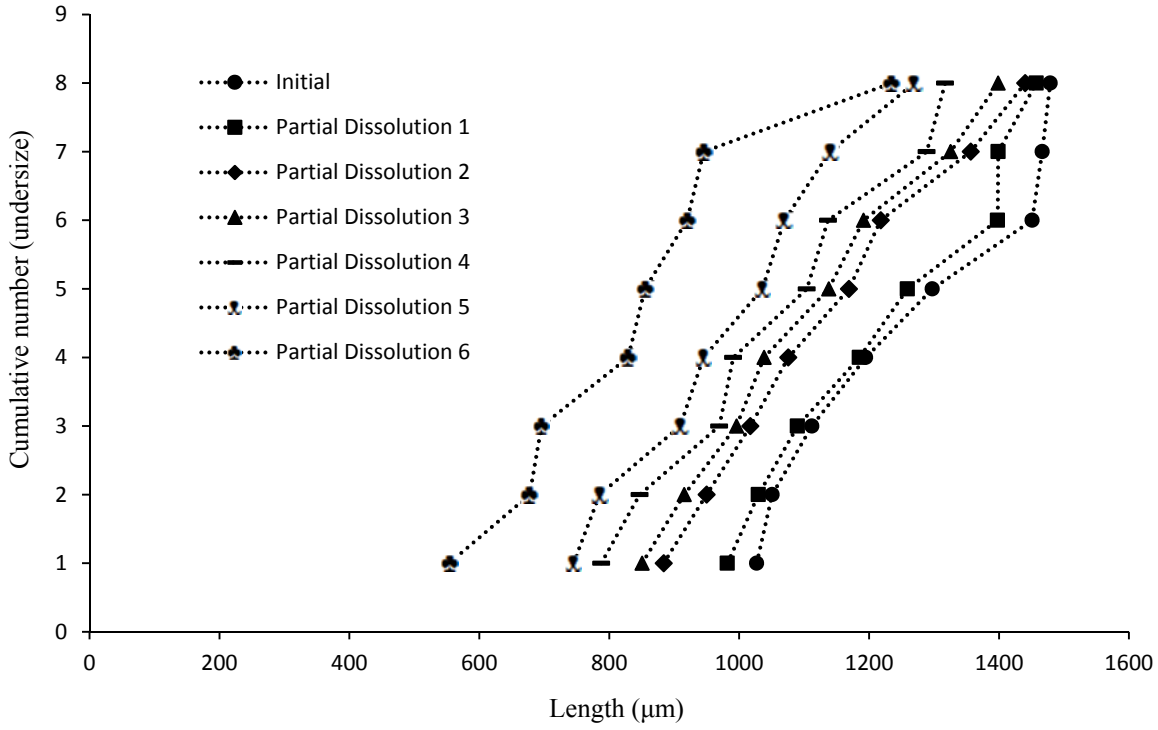


Figure S19. Chart comparing particle length versus the ranking of each particle in a partial dissolution series of **1** doped with 1.0 mol % of **3**.

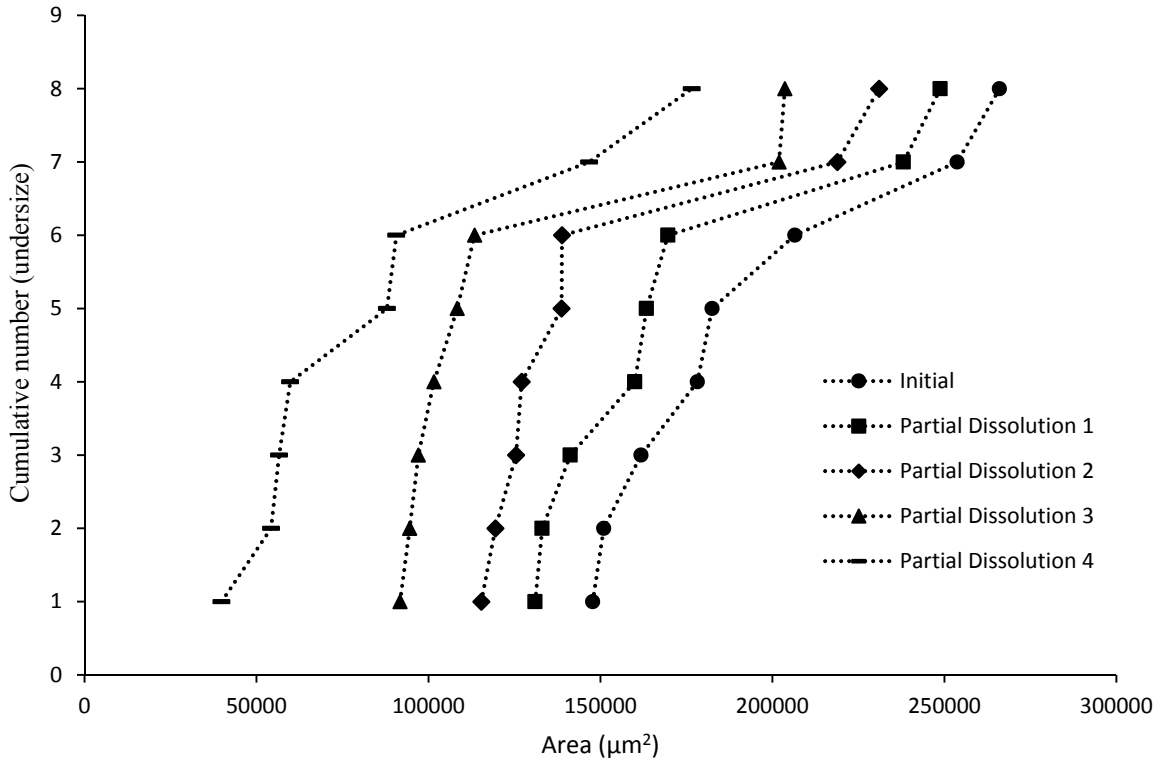


Figure S20. Chart comparing particle area versus the ranking of each particle in a partial dissolution series of **1** doped with 1.5 mol % of **3**.

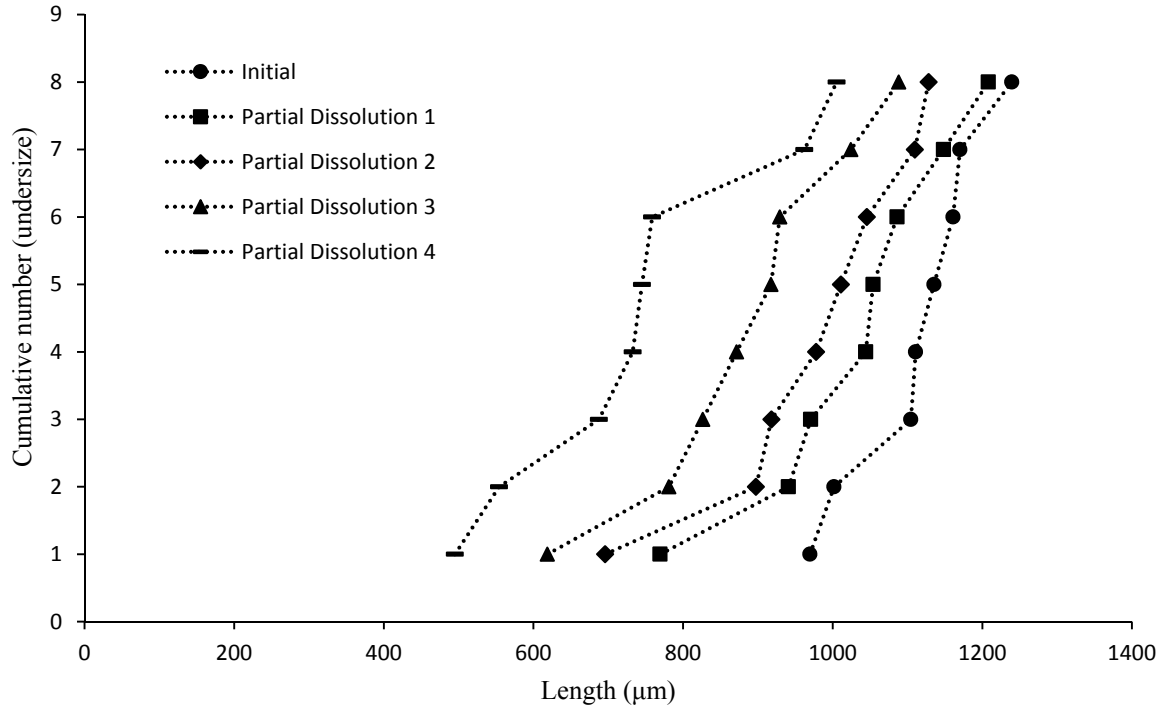


Figure S21. Chart comparing particle length versus the ranking of each particle in a partial dissolution series of **1** doped with 1.5 mol % of **3**.

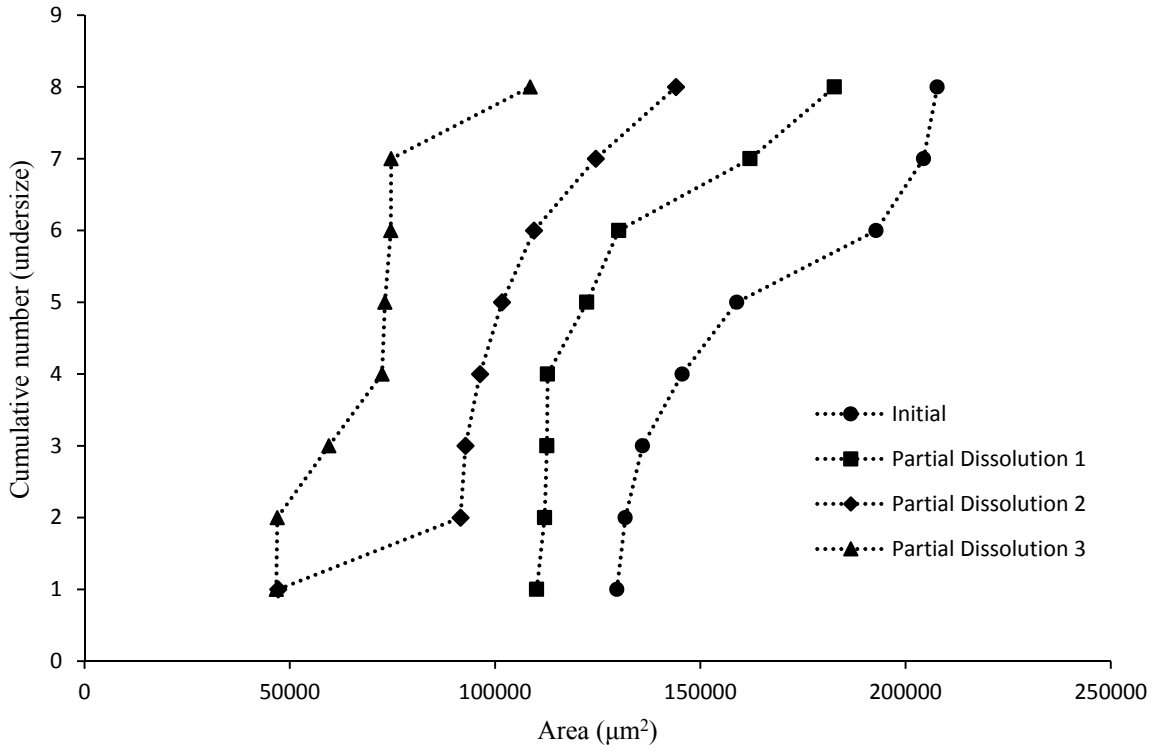


Figure S22. Chart comparing particle area versus the ranking of each particle in a partial dissolution series of **1** doped with 2.0 mol % of **3**.

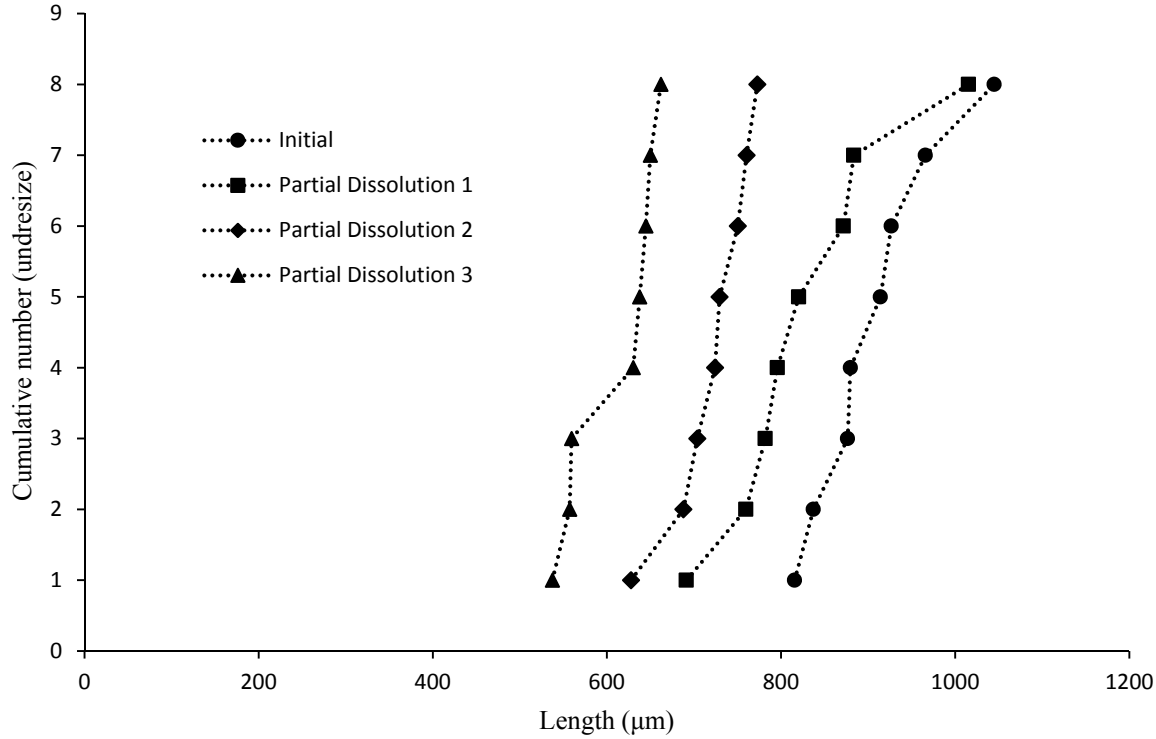


Figure S23. Chart comparing particle length versus the ranking of each particle in a partial dissolution series of **1** doped with 2.0 mol % of **3**.

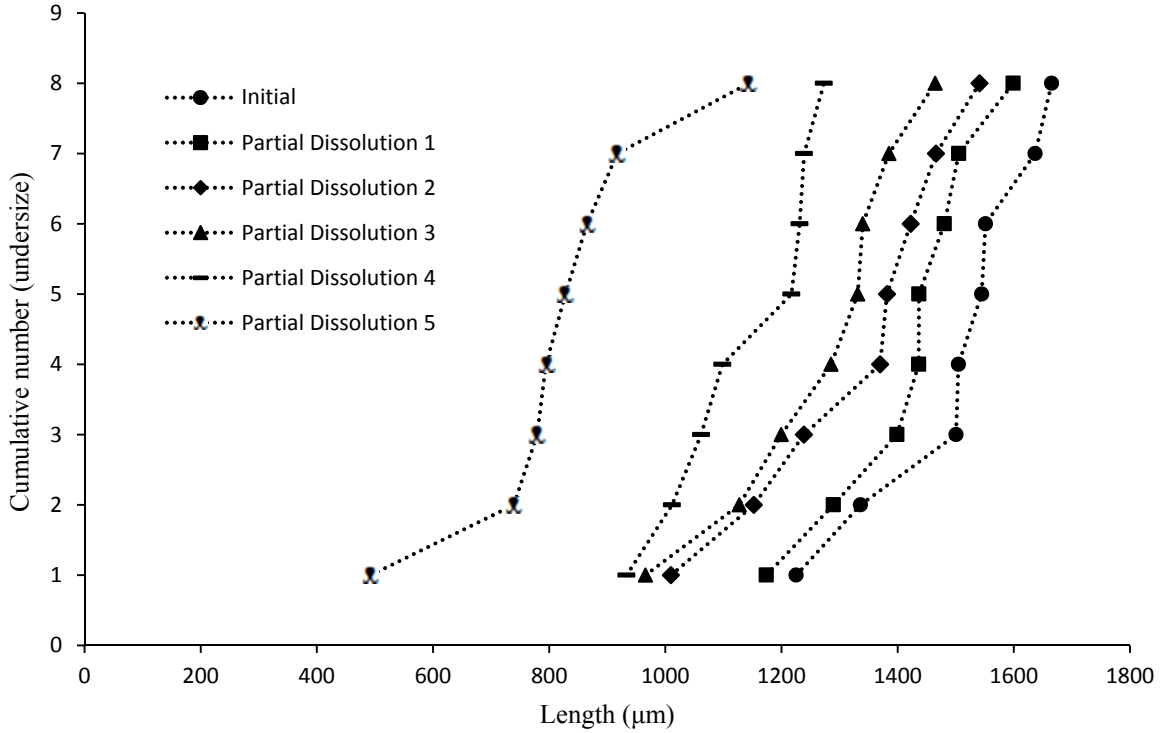


Figure S24. Chart comparing particle length versus the ranking of each particle in a partial dissolution series of **1** doped with 2.5 mol % of **3**.

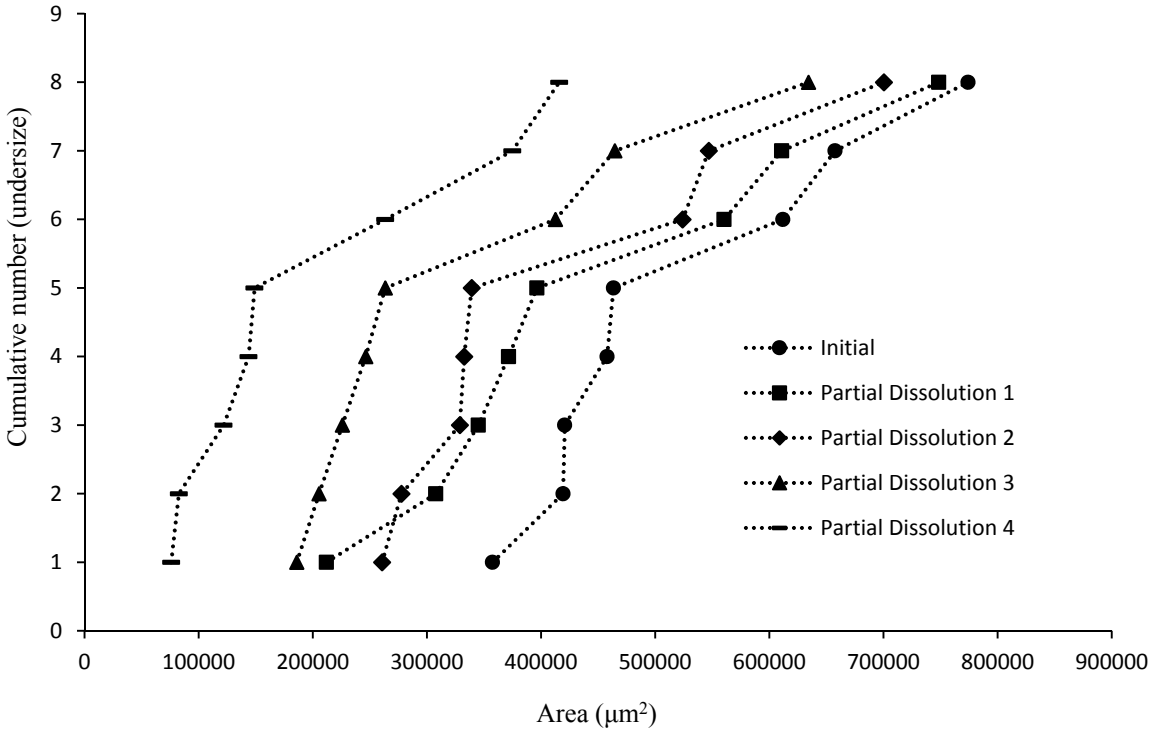


Figure S25. Chart comparing particle area versus the ranking of each particle in a partial dissolution series of **1** doped with 3.0 mol % of **3**.

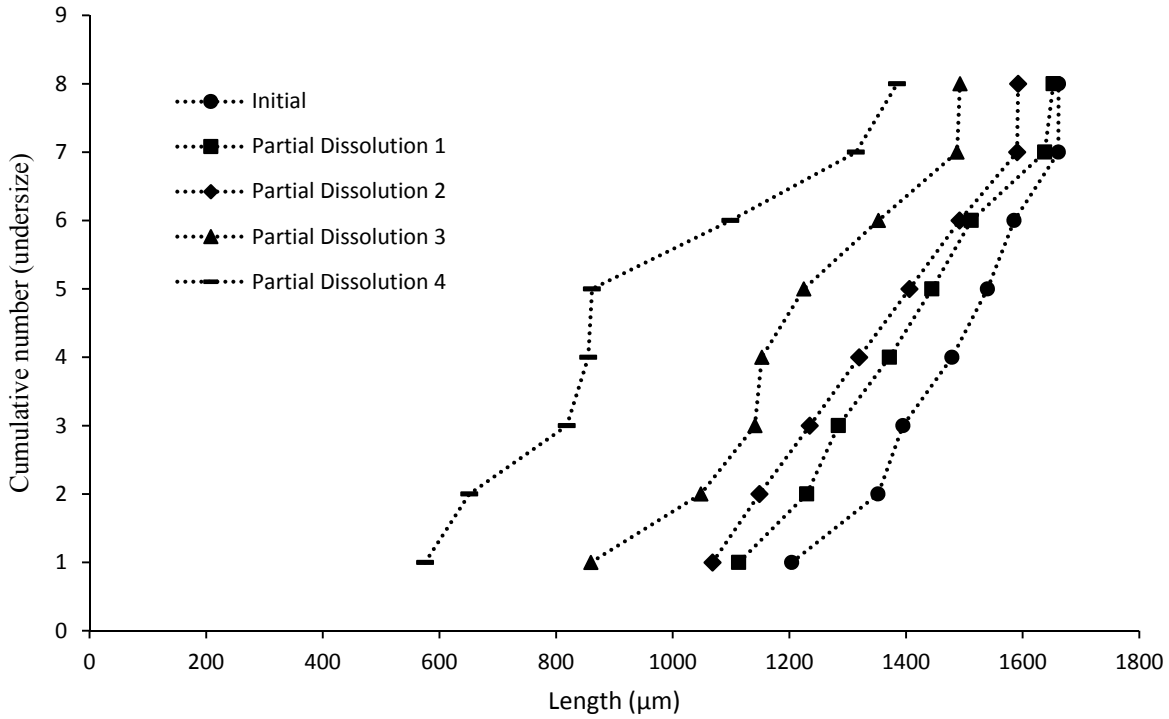


Figure S26. Chart comparing particle length versus the ranking of each particle in a partial dissolution series of **1** doped with 3.0 mol % of **3**.

%Impurity vs Dissolution mid-points% for the above

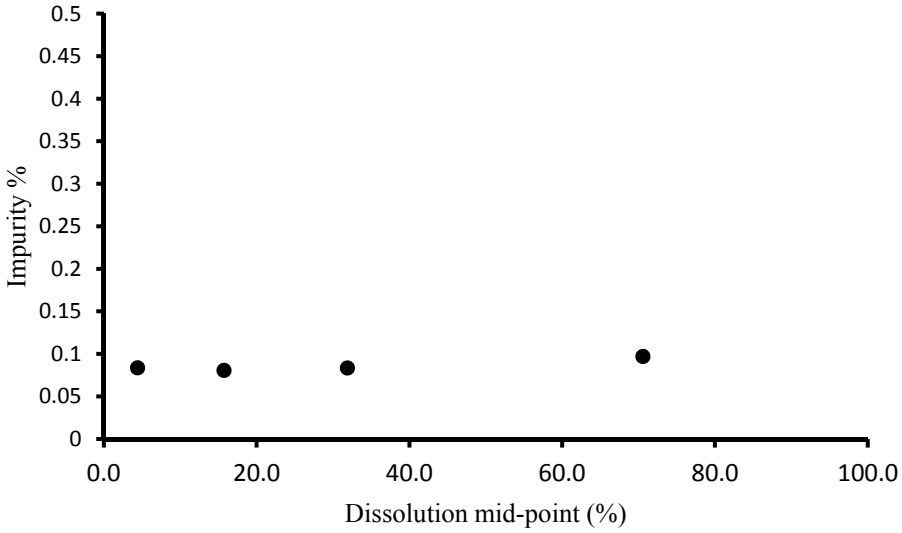


Figure S27. Plot of percentage by HPLC of added impurity in crystals of compound **1** *vs.* the dissolution mid-point for the sample of crystals grown from solutions containing 0.5 mol % of additive **2**.

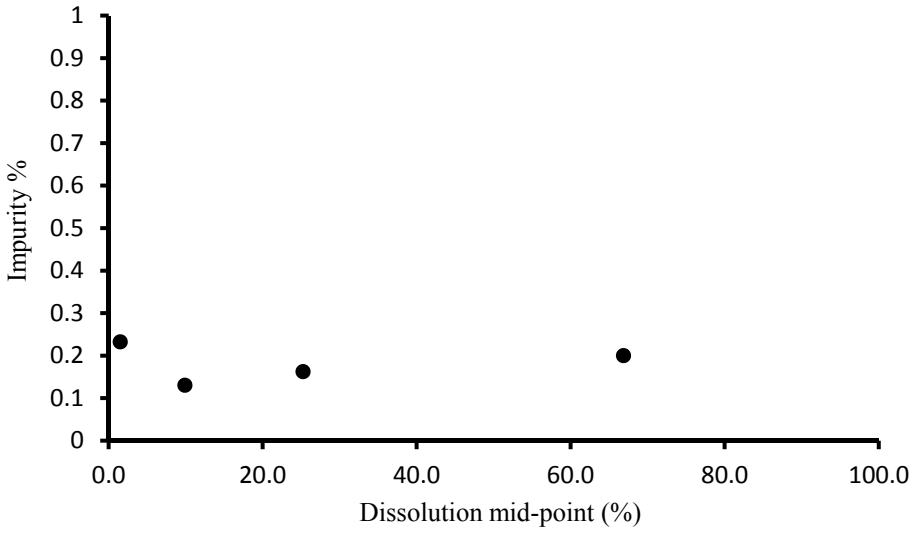


Figure S28. Plot of percentage by HPLC of added impurity in crystals of compound **1** *vs.* the dissolution mid-point for the sample of crystals grown from solutions containing 1.0 mol % of additive **2**.

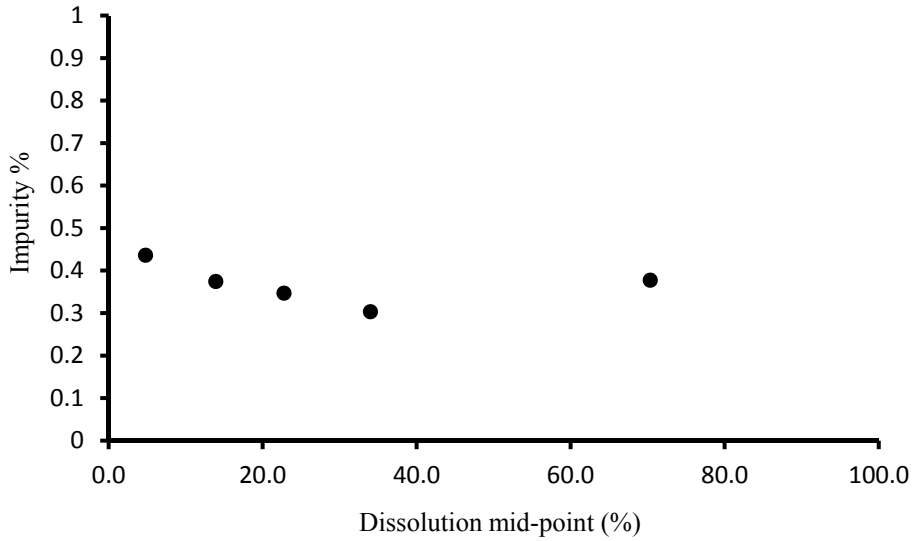


Figure S29. Plot of percentage by HPLC of added impurity in crystals of compound **1** *vs.* the dissolution mid-point for the sample of crystals grown from solutions containing 2.0 mol % of additive **2**.

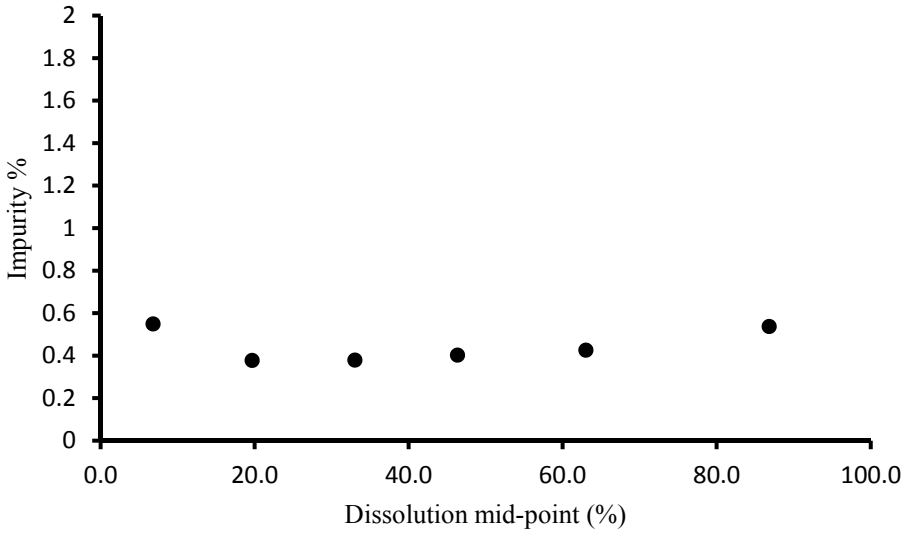


Figure S30. Plot of percentage by HPLC of added impurity in crystals of compound **1** *vs.* the dissolution mid-point for the sample of crystals grown from solutions containing 2.5 mol % of additive **2**.

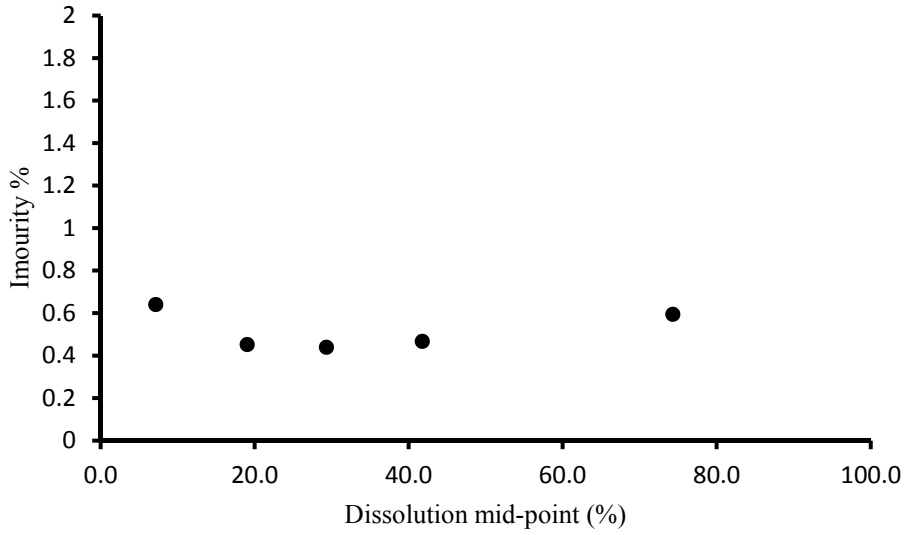


Figure S31. Plot of percentage by HPLC of added impurity in crystals of compound **1** *vs.* the dissolution mid-point for the sample of crystals grown from solutions containing 3.0 mol % of additive **2**.

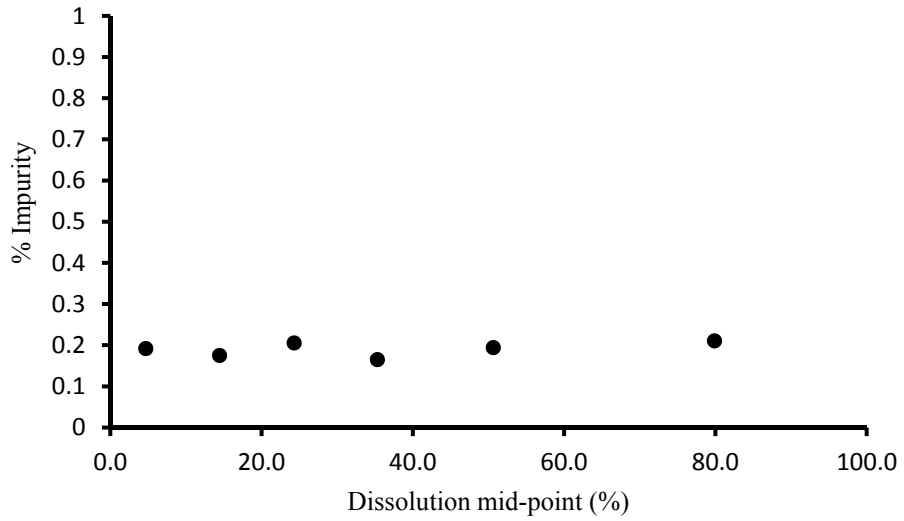


Figure S32. Plot of percentage by HPLC of added impurity in crystals of compound **1** *vs.* the dissolution mid-point for the sample of crystals grown from solutions containing 0.5 mol % of additive **3**.

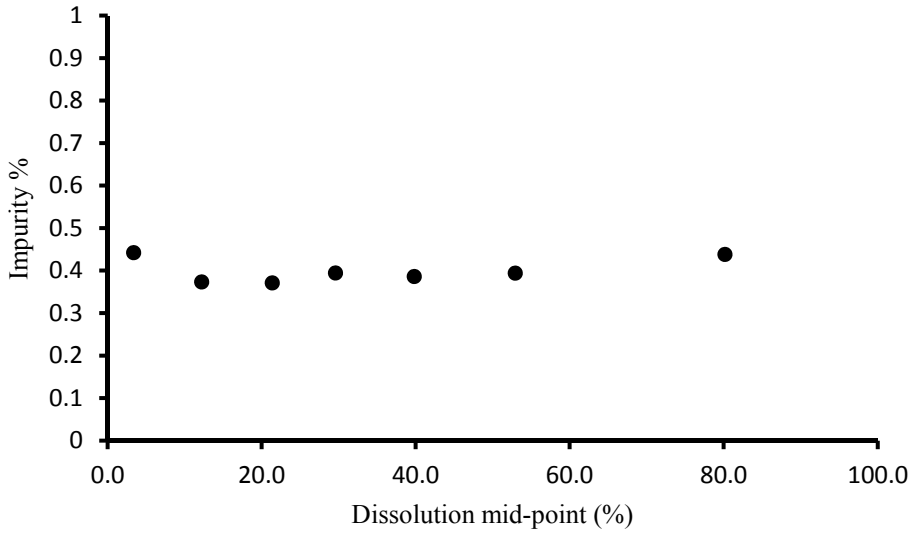


Figure S33. Plot of percentage by HPLC of added impurity in crystals of compound **1** *vs.* the dissolution mid-point for the sample of crystals grown from solutions containing 1.0 mol % of additive **3**.

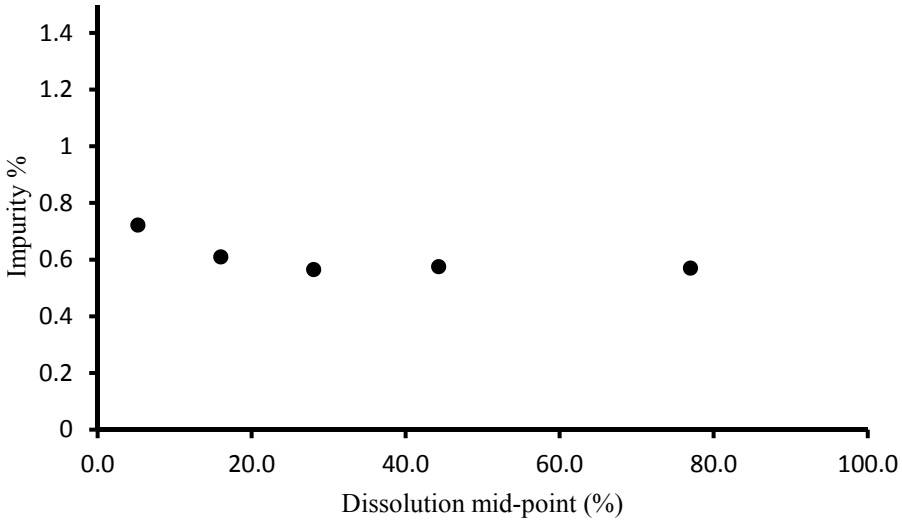


Figure S34. Plot of percentage by HPLC of added impurity in crystals of compound **1** *vs.* the dissolution mid-point for the sample of crystals grown from solutions containing 1.5 mol % of additive **3**.

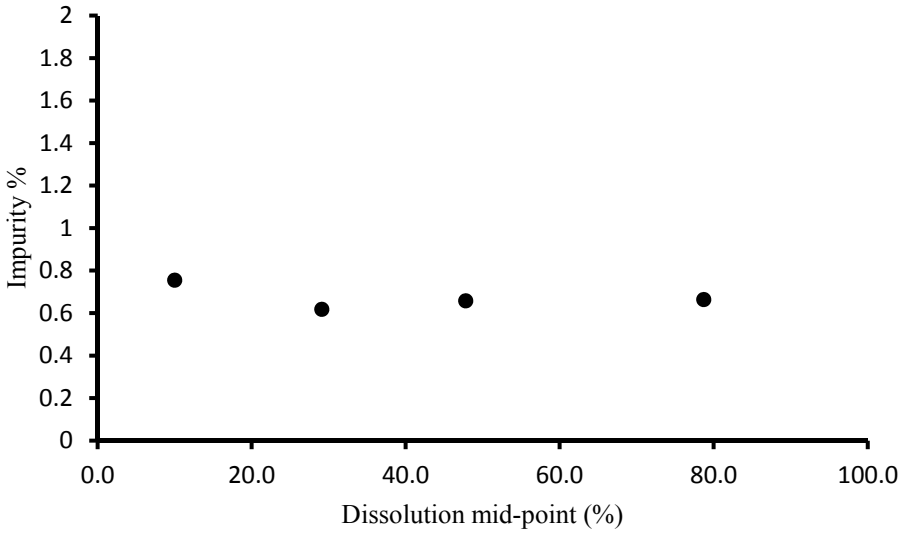


Figure S35. Plot of percentage by HPLC of added impurity in crystals of compound **1** *vs.* the dissolution mid-point for the sample of crystals grown from solutions containing 2.0 mol % of additive **3**.

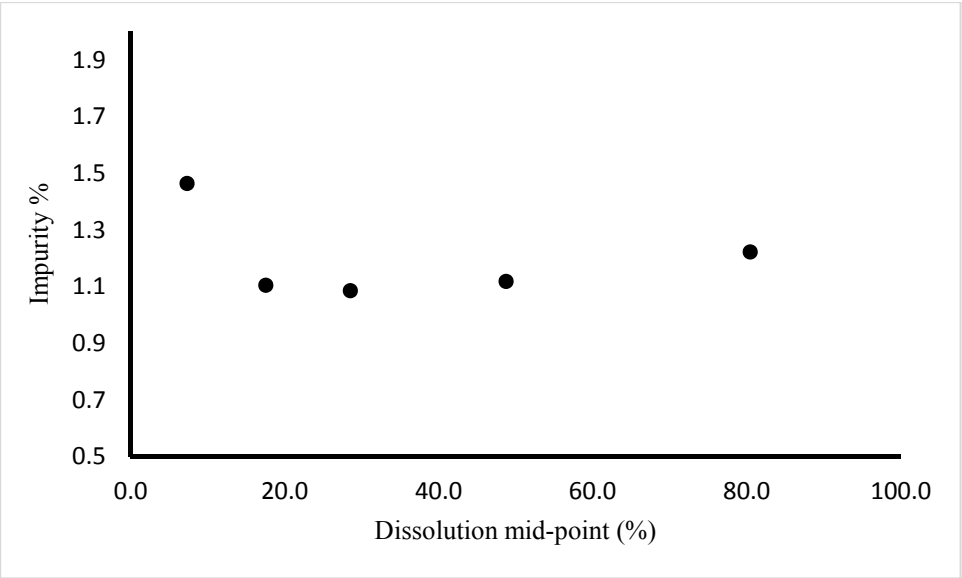


Figure S36. Plot of percentage by HPLC of added impurity in crystals of compound **1** *vs.* the dissolution mid-point for the sample of crystals grown from solutions containing 3.0 mol % of additive **3**.

Data from dissolution of single crystal grown from solution containing 3.0 mol % **3**.

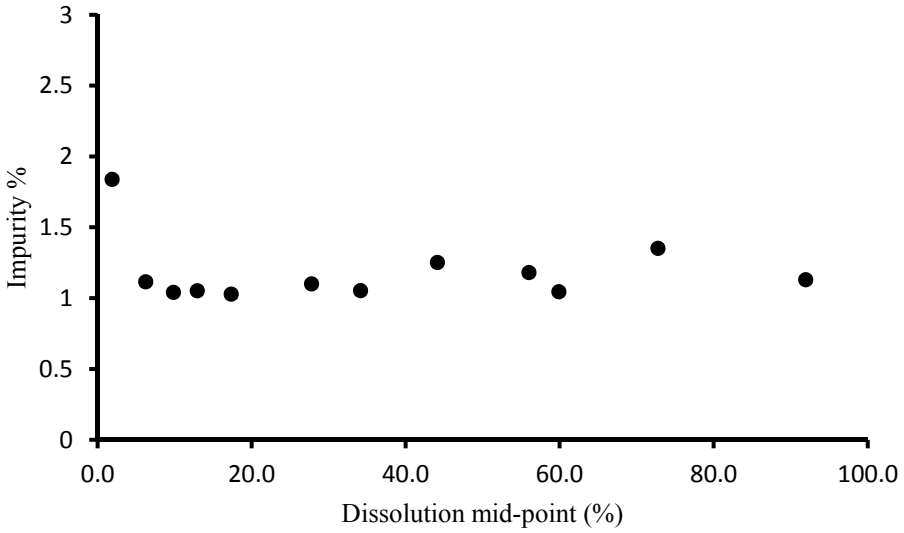


Figure S37. Plot of percentage by HPLC of added impurity in a single crystal of compound **1**, grown from solutions containing 3.0 mol % of additive **3**, *vs.* the dissolution mid-point for the crystal.